Model Calculations for Diffuse Molecular Clouds

by

A. E. Glassgold and William D. Langer

New York University

New York, New York 10003

Received _____

ABSTRACT

A steady state isobaric cloud model is developed. The pressure, thermal, electrical, and chemical balance equations are solved simultaneously with a simple one-dimensional approximation to the equation of radiative transfer appropriate to diffuse clouds. Cooling is mainly by CII fine structure transitions, and a variety of heating mechanisms are considered. Particular attention is given to the abundance variation of H_2 using an extension of the work of Hollenbach, Werner, and Salpeter. Inhomogeneous density distributions are obtained because of the attenuation of the interstellar UV field and the conversion from atomic to molecular hydrogen. The effects of changing the model parameters are described and the applicability of the model to OAO-3 observations is discussed. Good qualitative agreement with the fractional H_2 abundance determinations has been obtained. The observed kinetic temperatures near 80° K can also be achieved by grain photoelectron heating. The problem of the electron density is solved taking special account of the various hydrogen ions as well as heavier ones. The roles of CI and CII column density determinations are also emphasized.

I. Introduction

Observational information on interstellar clouds is rapidly increasing to such an extent that significant tests of theoretical models now seem feasible. We have recently presented a preliminary discussion (Glassgold and Langer, 1973c) of the H_2 and C abundances measured for 15 or so diffuse clouds with the Copernicus OAO-3 spacecraft (Spitzer et al, 1973; Morton et al, 1973). This article is the first relatively complete report of our work, and includes a full discussion of cloud properties and parameters as they relate to the OAO-3 results. In future publications we will discuss thicker clouds and other molecules besides H_2.

Our present model is basically a local steady state model in which all quantities vary from point to point except for the pressure (p_0), which is uniform. The inhomogeneities arise from the attenuation of the external radiations which heat, ionize, and dissociate the cloud constituents. The most important external radiation is the UV component of the interstellar radiation field. No doubt a steady state model is over idealized, but at least it permits a beginning to understanding how the many physical phenomena interact in interstellar cloud material. The isobaric condition should be appropriate if the sound crossing time is less than the mean lifetime of the cloud. For the OAO-3 clouds, the crossing time lies in the range 10^6 - 10^7 years.

The emphasis in this first report is on those components of an interstellar cloud which are most important for determining its thermal properties, i.e. the gas temperature T and density n. Thus we include the balance between H and H_2 because hydrogen is the most abundant species, and the balance between CI and CII because carbon is the most important cooling agent at

the temperatures characteristic of diffuse clouds ($\sim 100^{\circ}$ K). The interstellar grains are also included because they significantly attenuate the interstellar UV radiation field, catalyze the formation of H_2, and possibly heat the gas via photoelectron emission. The electron density n_e is also calculated because the electrons play a basic role in many of the underlying atomic reactions. The chemical equilibrium for calcium is included since it is relevant to determinations of n_e from measurements of the column densities of CaI and CaII (White, 1973 and references cited therein). Other constituents are not discussed here in detail, although our program has been constructed to deal with them. We have not attempted to analyze and to fit exhaustively the observations for any one particular cloud, but instead have concentrated on the general properties of the average cloud, represented by the ensemble of OAO-3 cloud observations.

One of our most important concerns is the heating of the clouds, since the cooling mechanisms for diffuse clouds seem to be fairly well established (Dalgarno and McCray, 1972). The problem here is to achieve relatively high temperatures in the neighborhood of 100° K (Hughes et al, 1971; Radhakrishnan et al, 1972; and Spitzer and Cochran, 1973). Although the observed C depletion (Morton et al, 1973) helps, significant grain photoelectron heating seems to be required, as advocated by Watson (1972).

Earlier work most closely related to this investigation is that of Hollenbach, Werner, and Salpeter (1971, referred to hereafter as HWS), who demonstrated quantitatively that H_2 will be concentrated in the interior of clouds by self-shielding of the dissociating UV radiation. HWS considered only the balance between UV dissociation of H_2 through the Lyman band lines (Solomon and Wickramasinghe, 1969) and formation on grains (Hollenbach and Salpeter, 1970) for constant total hydrogen density n and

temperature T. In this work we include the significant thermodynamic consequences of this balance and of the associated attenuation of the interstellar radiation field, as well as other chemical balances involving carbon, electrons, hydrogen ions, etc. The attenuation leads to significant inhomogeneities especially in n, which then feed back to affect the H_2 concentration.

In Section II we outline our calculations, and in Section III we describe the results obtained, which include the effect of varying the most important parameters and suggested ranges for them. A brief summary and some conclusions are given in Section IV.

II. Calculation

A. Overall Structure of the Calculation

We adopt a one-dimensional steady state model in which the density and column density of species X at position x are denoted respectively by n(X,x) and

$$N(X,x) = \int_0^x dx'\, n(X,x'), \tag{1}$$

x = 0 being the cloud surface. However, we usually suppress the x-dependence with the understanding that everything except pressure depends on x. In place of x we often use the total column density N of hydrogen to measure distance into the cloud

$$N = N(H) + 2N(H_2) \tag{2}$$

The radiation field intensity is $I(\lambda,x)$. Although the calculation involves a semi-infinite cloud medium, the treatment of the radiation

transfer discussed below is done so that finite-cloud effects are included in an approximate way.

The basic equations in the model are steady-state balances,

$$\underline{\text{pressure}}: \qquad \left[n_e(x) + \sum_X n(X,x) \right] kT = p_o \qquad (3)$$

$$\underline{\text{thermal}}: \qquad \Lambda(x) = \Gamma(x) \qquad (4)$$

$$\underline{\text{electrical}}: \qquad n_e(x) = \sum_X n_i(X,x) \qquad (5)$$

$$\underline{\text{chemical}}: \qquad P(X,x) = D(X,x) \qquad (6)$$

In these equations, $P(x)$ and $D(x)$ are respectively the production and destruction rates for X, $n_i(X,x)$ is the total ionic density for species X, and Λ and Γ are respectively the total cooling and heating rates. Effects of macroscopic motion and gradients are neglected. The local nature of these steady state balance equations has been emphasized by Eqs. (3)-(6). Each quantity also depends in principle on temperature T, on densities n(X), and on the radiation field I. Once I is known, there are just enough equations to solve for all densities n(X) and the temperature as a function of x and the pressure p_o. (If there are s species, there are s + 2 unknowns including n_e and T, and Eqs. (3)-(6) provide s + 2 equations since (6) is equivalent to s homogeneous equations.) Of course the radiation field $I(\lambda,x)$ depends on the solutions to (3)-(6) for all points x' such that $0 \leq x' \leq x$. Thus the solutions for the density and

temperature profiles $n(X,x)$ $n_e(x)$, $T(x)$ and the intensity $I(\lambda,x)$ must be obtained in a self-consistent manner.

B. Restricted Set of Balance Equations for Diffuse Clouds

By diffuse clouds we mean those with column densities to the center $N \leq 10^{21}$ cm^{-2} or with visual extinction $\lesssim 1$. The OAO-3 clouds fulfill this condition. Cosmic ray protons with energies as small as 2 MeV will hardly be attenuated by such clouds. On the other hand, the incident radiation field is significantly attenuated by the cloud material, especially in the far UV by the dust grains and H_2 molecules. As long as the temperature $T \lesssim 100^{\circ}$K, CII is the most effective of the atomic cooling agents. (The abundance of CI is too small to contribute significantly to cooling.) As for molecules, H_2 is not very effective (Glassgold and Langer, 1973a), and neither CO or HD are observed in sufficient abundance (Jenkins et al, 1973; Spitzer et al, 1973) to be competitive with CII (Glassgold and Langer, 1973a; Dalgarno and Wright, 1973). Thus the atomic species which determines the cloud structure are H, H_2, CI, CII, grains, and electrons. We now discuss their balance equations and those for Ca, which serves as a useful prototype for further applications of our model.

We do not consider the gain or loss of grain atoms, but simply specify the average grain area per gas atom inferred from the OAO-2 and 3 extinction measurements (Bless and Savage, 1973; York et al, 1973), i.e.,

$$\xi_{gr}(\lambda)\,\sigma_{gr}(\lambda) \equiv \frac{A_\lambda}{1.086\,N} \qquad (7)$$

Here $\sigma_{gr}(\lambda)$ is the mean total cross section of a grain for radiation of wavelength λ, and $\xi_{gr}(\lambda) = n_{gr}(\lambda)/n$ is the corresponding grain to gas density ratio, ignoring He and heavy atoms. In interpreting the extinction measurements, we replace the column density ratio N_{gr}/N by ξ_{gr}. Eq. (7) enters into the attenuation of the incident radiation and the catalysis of H_2 formation, both discussed in more detail below.

The formation and destruction of H_2 is treated along the lines of HWS, but cosmic ray destruction (Solomon and Werner, 1971) and the effects of ion molecule reactions are also included:

$$R_1 n(H) n = \left(\zeta_2(H_2) + \eta(H_2, I) \right) n(H_2) - \left(\frac{dn(H_2)}{dt} \right)_{\text{ion react}} \qquad (8)$$

On the left side we have production on grains with a rate constant

$$R_1 = 1/2 \; \gamma \; v_{th}(H) \; \frac{n_{gr}}{n} \; A_{gr} \qquad (9)$$

where γ is an efficiency factor (~ 0.3 for $T \simeq 100^{\circ}$ K, Hollenbach and Salpeter, 1970), $v_{th}(H)$ is the mean speed of impinging H atoms, n_{gr} is the total density of grains and A_{gr} their mean area for catalyzing H_2 formation. By adopting a "typical" grain model with $n_{gr} A_{gr}/n = 3.8 \times 10^{-22}$ cm^2, HWS estimated $R_1 \simeq 10^{-17}$ cm^{3}s^{-1}, fairly independent of temperature for $T \lesssim 100^{\circ}$ K. Much earlier, McCrea and McNally (1960) had estimated $R_1 \simeq 7 \times 10^{-17}$cm^3 s^{-1} by using

somewhat smaller and denser grains and the maximum efficiency $\gamma = 1$. On the other hand, the large far UV-extinction observed by OAO-2 and -3 imply from (7) values for $\xi_{gr}\,\sigma_{gr}$ as large as $3 \times 10^{-21} cm^2$ for the typical reddened star and $5 \times 10^{-21}\ cm^2$ for ζ Oph. These measurements seem to suggest a major component in the grain distribution (York et al, 1973) of small particles of linear dimension ~ 150 Å. If the corresponding area is assumed to be about as effective as the larger grains considered by HWS; then their estimate of R_1 should be revised upward to $\sim 5 \times 10^{-17} cm^3 s^{-1}$ for the typical reddened star (Spitzer and Cochran, 1973) and to $7 \times 10^{-17} cm^3 s^{-1}$ for ζ Oph. Because of the considerable uncertainty in these estimates, we have investigated a range for R_1 from $5 \times 10^{-18} cm^3 s^{-1}$ - $10^{-16} cm^3 s^{-1}$.

The right side of (8) contains the ionization rate ζ_2 by cosmic rays and the photo-dissociation rate η. Although direct dissociation of H_2 by protons with cosmic ray energies is unimportant, dissociation by primary electrons is not (Glassgold and Langer, 1973b). Close to 98% of the inelastic events produce $H_2^+ + e$ and 2% $H + H^+ + e$ (Adamcyzk et al, 1966). These reactions are summarized in the table of Appendix A. Because the low energy cosmic ray flux is not directly measured, we have considered a range for $\zeta_p(H)$, the primary ionization rate of atomic hydrogen, from $10^{-18} s^{-1}$ - $10^{-15} s^{-1}$. Photodissociation of H_2 below 13.6 eV requires a two-step process in which discrete line excitation is followed by dissociation (Solomon in Field et al 1966). The rate $\eta(H_2, I)$ will depend on the values of $I(\lambda, x)$ at appropriate wave lengths in the range from 1108 Å - 912 Å, which

depend sensitively on position x. Our calculation is based on the method given in the appendix of HWS, and will be discussed briefly later. For a very thin cloud and Habing's (1968) field, we obtain $\eta_o = 0.44 \times 10^{-10} s^{-1}$.

Equation (8) also contains a term arising from ion-molecule, charge-exchange, and dissociative recombination reactions of the cosmic ray produced ions H_2^+ and H_3^+. These reactions are important for heating and ionizing molecular clouds (Glassgold and Langer, 1973a,b), and for the production of heavier molecules (Watson, 1973; Herbst and Klemperer, 1973; Dalgarno, Oppenheimer, and Berry, 1973). The term $\left(\frac{dn(H_2)}{dt}\right)_{\text{ion react}}$ in (8) is of the order of magnitude of $\zeta_2 n(H_2)$, and becomes important only when $\eta \leq \zeta_2$. These reactions are incorporated in our program, and we discuss them below in Appendix A in connection with the electrical balance equations. The gas density n, excluding He and heavy atoms, is the hydrogen mass density in units of m_h.

$$n = n(H) + 2n(H_2). \tag{10}$$

When $\left(\frac{dn(H_2)}{dt}\right)_{\text{ion react}}$ and $\zeta_2 n(H_2)$ are ignored, the fraction of hydrogen mass in molecular form is

$$f \equiv \frac{2n(H_2)}{n} = \left(1 + \frac{\eta}{R_1 n}\right)^{-1}. \tag{11}$$

The chemical balances for C, Ca and other heavy atoms are determined by the familiar relations (Spitzer, 1968):

$$\frac{n(X_{r+1})}{n(X_r)} = \frac{G(X_r)}{\alpha(X_{r+1})n_e} \quad , \tag{12}$$

where α is the radiative recombination rate coefficient and G is the photo ionization rate

$$G(X_r,x) = \int_{912\ \mathring{A}}^{\lambda_{th}(X_r)} d\lambda\ \sigma_i(X_r,\lambda) \left[c_{cont}(x)\, I(\lambda,x)\right] \quad . \tag{13}$$

Cosmic ray ionization has been ignored. In (13), σ_i is the photo ionization cross section and c_{cont} is a renormalization factor converting intensity to flux discussed below. For CI and CaII, σ_i may be replaced by their threshold values, whereas for CaI the complete observed cross section (Carter et al, 1971) increased by an overall factor of 2 (McIlrath and Sandeman, 1972) is used. The values needed to evaluate (12) for n(CII)/n(CI), n(CaII)/n(CaI), and n(CaIII)/n(CaII) are given in Table 1, as are values of G/α at zero optical depth for a very diffuse cloud. The reduction in G/α by UV attenuation is included in our calculations; the method for treating the attenuation is discussed below. In addition to (12), we have the total abundance of species X

$$n(X) = \sum_r n(X_r) \ , \tag{14}$$

and the relative abundance

$$\xi(X) = n(X)/n \tag{15}$$

We consider only CI, CII, CaI, CaII, CaIII because $\lambda_t(\text{CIII}), \lambda_t(\text{CaIV}) < 912\text{Å}$. In accord with the preliminary OAO-3 C-depletion determinations (Morton et al, 1973), we consider values for ξ (C) in the range from 10^{-5} - 10^{-4}. Although Ca is generally underabundant, we do not concern ourselves with choices of ξ (Ca) since CaIII (and thus the total Ca abundance) is not measured; also Ca does not affect the thermodynamic structure of the cloud.

The ion densities required to evaluate the electron density n_e from (5) may be classified into two main groups, those of the light atoms (H and He) and those of the heavy atoms (O, C, N, etc.). In our model, the ionizing agents are low energy cosmic rays and the stellar radiation field cut-off short of 912 Å. This type of radiation field can not ionize the light atoms, but cosmic rays will ; with characteristic rates which we take to be in the range $10^{-18}s^{-1}$ - $10^{-16}s^{-1}$. The radiation field ionizes heavy atoms with ionization potentials I < 13.598 eV with a characteristic rate $\Gamma_i \sim 10^{-10}s^{-1}$ for diffuse clouds. Despite significant attenuation in the far UV, photo ionization is the most important ionization mechanism in our model for such heavy atoms as C, Mg, Si, etc., in gross qualitative agreement with OAO-3 cloud abundance determinations (Morton et al, 1973).

All the ions recombine radiatively with characteristic rate coefficient $\alpha \simeq 7 \times 10^{-12} (T/100)^{-0.7}$ cm^3s^{-1} except for the molecular ions. The cosmic ray produced H_2^+ ions are rapidly transformed into H_3^+ ions and then recombine dissociatively, i.e.,

$$p + H_2 \rightarrow H_2^+ + e + p' \qquad (16.a)$$

$$H_2^+ + H_2 \rightarrow H_3^+ + H \qquad (16.b)$$

$$H_3^+ + e \rightarrow H_2 + H \text{ and } 3H \qquad (16.c)$$

The detailed analysis of ion densities in Appendix A shows $n(H_2^+)$, $n(H_3^+) \ll n_e$. This is to be expected from the very large rate coefficients for (16.b): $K_2 = 2 \times 10^{-9} cm^3 s^{-1}$ (Trujillo and Neynaber, 1968; Bowers et al, 1969) and for (16.c): $\beta_3 = 4 \times 10^{-6} T^{-\frac{1}{2}} cm^3 s^{-1}$ (Leu et al, 1973). The balance equations for the heavy atoms were already given in (12), and a complete study of the ionization balance is carried out in Appendix A. In our program we use the results(A-30)-(A-40), which apply if $N < 10^{21} cm^{-2}$ and $x_e \lesssim 0.1$. Our result for the electron concentration becomes relatively simple if n(CII) >> n(CI):

$$x_e = 1/2 \left(\xi_{HA} + \sqrt{\xi^2_{HA} + 4 \zeta'/n \alpha(H^+)} \right), \qquad (17)$$

where ξ_{HA} is the abundance of ionized heavy elements,

$$\xi_{HA} = \sum_{\substack{X \\ I(X) < I(H)}} \xi(X) \qquad (18)$$

and

$$\zeta' = \left\{ \zeta_1 + 1/2\ \zeta_2(H_2^+) \left[\frac{K_1 f}{K_1 + (K_2/2 - K_1) f} \right] \right\} (1-f)$$

$$+ 1/2\ \zeta(H^+) f + \xi(He)\ \zeta(He) \frac{\alpha(H^+)}{\alpha(He^+)} \qquad (19)$$

is an effective cosmic ray ionization rate. The reaction rates K_1 and K_2 are given in Table A and $\xi(He) = 1/14$ (Cameron, 1973); also $\alpha(He^+) \approx \alpha(H^+)$ (Seaton, 1951).

The dominant contribution to (18) is expected to come from C. Most heavy elements are observed to be significantly depleted in the OAO-3 clouds, but there is some uncertainty whether $\xi(N)$ should be included in (18) (Morton et al, 1973). The maximum value of ξ_{HA} obtained from solar abundances is 6×10^{-4}, but the observed depletion (Morton et al, 1973) suggests the range 5×10^{-5} - 1×10^{-4}, with the smaller number representing overall depletion by 10 and no NII. For OAO-3 clouds, we might use the parameters ($1 - f = 1$, $\alpha = 6.4 \times 10^{-12} cm^3 s^{-1}$, $n \approx 25\ cm^{-3}$) to characterize the surface region, and ($1 - f \approx 0.2$, $\alpha = 8.3 \times 10^{-12} cm^3 s^{-1}$, $n = 50\ cm^{-3}$) for the interior of the largest clouds; the corresponding values of x_e are respectively 8×10^{-4} and 2.5×10^{-4} when $\zeta_p(H) = 10^{-16} s^{-1}$. As a result of depletion, cosmic rays will be the dominant ionization mechanism in diffuse clouds even if $\zeta_p(H)$ is as small as $10^{-17} s^{-1}$.

C. The Interstellar UV Field and Its Attenuation

The thermodynamic structure of interstellar clouds is strongly affected by the interstellar radiation field in the band from 912 Å to 1101 Å, the ionization threshold for CI. The Lyman band lines begin at 1108 Å, although the ones important for dissociation do not occur until 1026 Å ($\nu' = 6 \leftarrow \nu = 0$). The radiation field down to 2028 Å is also required for the chemical balance of Ca.

In discussing the intensity $I(\lambda, x)$ as a function of wavelength λ, we ignore reradiation by both grains and H_2 molecules at wavelengths $\lambda' > \lambda$. This would be a serious error if we were treating the

population distribution of the molecules or the thermal properties of the grains, but we believe that such effects are not important in considering the total H_2 abundance. This is in accord with earlier work by HWS; Black and Dalgarno (1973) have recently considered the effects of the fluorescent radiation on the population of the H_2 molecules. Elastic scattering by H_2 molecules is ignored, whereas elastic scattering by grains is assumed to occur mainly in the near forward directions. We thus adopt a transfer model in which each wavelength λ is individually attenuated by the H_2 Lyman band lines and the grains. Because the line absorption is fundamentally different from the grain continuum absorption, we have two distinct phenomena to discuss.

There are other sources of line and continuum absorption, but the 60 Lyman lines ($v' = 0 - 19 \leftarrow v'' = 0$) and the grains are the most important in the spectral range of interest. Because of the low abundance of heavy atoms and the much higher-frequency absorption lines of He, the only real contenders for overlapping lines are the Lyman series of H and the Werner bands of H_2. The probability of overlap is increased by the fact that considerable absorption is occurring in the radiative wings of the lines, i.e. the lines have an effective width $\Delta\nu \propto (fN)^{\frac{1}{2}}$ where f is the oscillator strength. We find that L_β and L_γ shield the $R_{6 \leftarrow 0}(1)$ - 1024.98 Å and $R_{11 \leftarrow 0}(0)$ - 971.99 Å transitions, respectively. (We use the standard notation for the $X \rightarrow B$ and $B \rightarrow X$ Lyman band transitions:

$\nu'J' \leftarrow \nu J$ and $\nu'J' \rightarrow \nu''J''$ or K'', depending on whether dissociation occurs or not.) Momentarily assuming a constant UV flux in the 1025 Å - 925 Å band where most of the dissociation occurs, we estimate that these two lines would contribute only 2.7% of the dissociations. Because of the reduced oscillator strengths for both the Lyman series and Lyman band lines near the former's limit, shielding of the upward transitions $\nu' \leftarrow 0$ for $\nu' \lesssim 19$ is probably not effective for OAO-3 clouds. Moreover, the three components of $19 \leftarrow 0$, which are nearly coincident with Lyman lines near the series limit, contribute only 1% of the dissociations. The predicted decrease in UV flux in this region (Jura, 1974) also implies a further reduction in the role of these lines. Thus the overlapping Lyman series reduces the dissociation rate by only $\sim$ 3%, which is negligible. Overlap with the Werner bands also appears to be unimportant in this context, there being only one near coincidence. The Werner bands accessible with radiation from 912 - 1009 Å have negligible dissociation probabilities (Stephens and Dalgarno, 1972). The photoionization of heavy atoms does not appear to be an important attenuator of the UV continuum below 2000 Å because of their depletion and the large grain cross section associated with the $1/\lambda$ extinction. The most abundant heavy atoms with $I < 13.6$ eV, Mg, Si, Fe, and S, have a total solar abundance of $\sim 10^{-4}$ and a very uncertain average photoionization cross section $\sim 10^{-17} cm^2$. Assuming depletion by $\sim 10^{-1}$, they contribute an attenuation cross section of $\sim 10^{-22}$ cm^2 per gas atom as compared with $2 \times 10^{-21} cm^2$ from grains.

As mentioned earlier, our treatment of the Lyman band line photo dissociation of H_2 follows closely that described in the appendix of HWS, so we only mention a few important changes. As in HWS, we assume that the H_2 molecules are in the ground electronic state with $\nu = 0$, $J = 0$ and 1. This low state of excitation seems to apply to most but not all of the OAO-3 observations (Spitzer and Cochran, 1973). We have included the possibility of arbitrary populations P_J for the two ground states, but have found the calculated abundance of H_2 to be insensitive to whether P_J is given by the high temperature limit $P_1/P_0 = 3$ used by HWS or by the observations of Spitzer et al (1973), which correspond to an excitation temperature of $\sim 80^\circ$ K. In contrast to HWS we treat all of the 60 accessible Lyman band lines on an individual basis. Upward absorption and downward dissociation probabilities are taken from Allison and Dalgarno (1969) and Dalgarno and Stephens (1972), respectively. The latter correspond to a mean dissociation probability per H_2 molecule of 0.26 in an optically thin region, which is $\sim 2/3$ the older value used by HWS. We have considered Doppler shift parameters $b_D = (2\overline{v_r^2})^{\frac{1}{2}}$ in the range from 1-10 km/s, the lower value being the one used by HWS and characteristic of thermal broadening at 100° K. The H_2 abundance near the surface of a cloud is very sensitive to b_D, as may be seen from Fig. 2. Values near 4 km s^{-1} seem to be appropriate to the OAO-3 clouds (Spitzer et al, 1973, and private communication).

Our treatment of the attenuation of the UV continuum is based on the OAO selective extinction measurements, as already mentioned above in connection with the role of the dust grains in catalyzing H_2 formation. The extinction A_λ, required in (7) for the mean total cross section at λ per gas atom, is obtained from the selective extinction measurements $E_{\lambda-V}/E_{B-V}$ through the relation

$$\frac{A_\lambda}{A_V} = 1 + \frac{1}{R} \frac{E_{\lambda-V}}{E_{B-V}} \quad . \tag{20}$$

For the general extinction we use R = 3, in accord with the discussion by Bless and Savage (1972). We have adopted a constant albedo a = 1/2. Witt and Lillie (1973) have deduced values of a from measurements of the diffuse galactic light which rise rapidly as λ decreases from 2000 Å to 1500 Å. It is difficult to comprehend such large values on the basis of reasonable grain models, and so for our present model calculations we have adopted a "dark grey" grain scattering picture with a = 1/2. The absorption cross sections $\sigma_{gr\ abs}(\lambda)$ used here are given in Fig. 1 for the "average" extinction curve of Bless and Savage (1972) extended by OAO-3 measurements (York et al, 1973). To indicate the deviations possible, cross sections obtained on the same basis for ζ Oph are also given.

In line with our objective of obtaining an overall picture of diffuse clouds, we have used incident radiation fields characteristic

of some typical or average location in the interstellar medium. The same isotropic intensity $I_0(\lambda)$ characterizes the field at every point on the surface of the cloud, and we assume that the material inside the cloud has the same macroscopic velocity and Doppler parameter b_D. These restrictions might well have to be relaxed in attempting an interpretation of observations toward a particular star. In particular, proximity of a cloud to a star can cause a large increase in $I_0(\lambda)$, as is documented by Herbig's calculation (1968) of photoionization coefficients for ζ Oph and Jura's calculations (1974) of fluxes for OAO-3 stars. At the start of this work there were no calculations of the average galactic radiation field which adequately covered the entire spectral range from 912 Å to 2028 Å. Thus we interpolated on Habing's calculations (1968), extrapolated Lillie's data (1968) below 2000 Å, extrapolated Witt and Johnson's calculation (1973) below 1330 Å, and most recently extrapolated Jura's calculation (1974) below 1125 Å, to obtain the four curves in Fig. 2. Many of the illustrative calculations given below use curve 2, since Habing's field has been used by so many other authors.

The intensity is attenuated in our model according to the formula

$$I(\lambda,x) = I_0(\lambda)e^{-\tau_\lambda(x)} \quad , \qquad (21)$$

where the optical depth at a distance x into the cloud $\tau_\lambda(x)$ is the sum of optical depths due to absorption by grains and H_2

molecules. We use (21) in such a way, however, as to take into account approximately the fact that radiation can reach the point x from any direction for a finite cloud. In particular, the intensity is converted into an effective flux $F(\lambda,x)$ for absorption

$$F(\lambda, x) = c\, \pi\, I\, (\lambda, x)\ , \qquad (22)$$

with c chosen separately for the lines and for the continuum. When this is done, it is possible to use the method devised by the appendix of HWS for treating the dissociation of H_2 and to treat also the pressure, thermal, electrical, chemical balance relations (3) - (6). Values for c_{cont} and c_{line} were chosen on the basis of exact solutions of radiative transfer problems (without scattering) for slabs and spheres, the former restricted to absorption coefficients symmetric about the mid plane and latter to constant absorption coefficients. These solutions involve exponential integrals as well as simple exponentials, and depend on the distance from the surface measured by τ and the size as measured by the optical depth τ_o to the center (λ is suppressed here). For a given τ_o or a range of τ_o, one can choose c so that the difference between the absorption calculated from (22) and from the exact solution is minimized. For the Lyman band lines, for which $\tau_o \gg 1$ as long as $N > 10^{19} cm^{-2}$, $c_{line} = 1$ gives very high accuracy independent of whether a slab or sphere solution is used. For the continuum, where $\tau_o \lesssim 1$, there are important differences between the two geometric models. Of course we generally do not know the geometry of diffuse clouds,

which might actually be quite different from either of the two simple cases we've treated. Furthermore, even if a cloud were approximately spherical, we would not know the line-of-sight intersection. For OAO-3 clouds with considerable H_2 abundance $c_{cont} \tilde{=} 2$ and 3 respectively for slab and sphere. Using fixed values for c_{cont} leads to errors in the radiation transfer which are typically of the order of 10%, but as much as 25% near the surface. These are considerably less than the differences in the solution between the extreme geometrical forms which might be possible for interstellar clouds. In most of our examples discussed below, we use $c_{cont} = 3.0$, but also consider the effects of varying c_{cont} from 1-4, i.e. the range from very thick to very thin clouds (see Fig. 3).

(INSERT PAGE 21a.)

D. Heating and Cooling

As mentioned earlier, CII is the most important cooling agent for diffuse clouds. Because the theory of the cooling by CII and the other contributing coolants is extremely familiar (see for example the review by Dalgarno and McCray, 1972), we omit any detailed discussion of this process. We should mention, however, that the cooling rates are proportional to the relevant abundances so that depletion reduces them, thus tending to produce higher temperatures (Field et al, 1969; Meszaros, 1972). Further, the column densities of the heavy atoms and ions in diffuse clouds are small enough so that there is negligible trapping of cooling radiation.

There is much less certainty as to the means by which the interstellar clouds are heated. We have recently published a

(INSERT)

It is, of course, possible to treat the radiation problem for spherical geometry by solving numerically for $I(\lambda,x,\Omega)$ in the manner of HWS. Exact solutions can also be found for a slab. We have chosen to work with the approximate solution (21) and (22) (a corrected semi-infinite slab) because it allows us to calculate models for clouds of varying total column density in one computational run. In addition, we have chosen to investigate the effects of varying many of the input parameters, which is only feasible with the efficient numerical techniques associated with our sample model.

detailed study of the heating and ionization of an H_2 gas by cosmic ray protons and by soft X-rays (Glassgold and Langer, 1973b) which can easily be applied to the presently considered diffuse clouds containing a mixture of H and H_2. First of all, the X-rays can not penetrate beyond a thin surface layer of the cloud since the column density corresponding to an absorption optical depth of unity is

$$N_{1_{XR}} \simeq 2 \times 10^{19} \text{ cm}^{-2} \left(\frac{100 \text{ eV}}{E_{XR}} \right)^3 .$$

Within this distance, the observed soft X-ray flux down to $E_{XR} = 100$ eV would produce an ionization rate $\zeta_{XR} \sim 3 \times 10^{-16} s^{-1}$ and a heating efficiency of $\sim 1/3$. Although these X-rays may have some observational consequences, we ignore them in our model since they are inoperative throughout the bulk of the clouds under consideration, which have column densities to the center ranging from $N = (1 - 10) \times 10^{20} \text{cm}^{-2}$. Despite qualitatively different features for the interaction of secondary electrons with H_2, the calculated heating and ionization rates are not very much different than for H. The heating Q and number of electrons produced per primary ionization event ϕ for a 2-MeV proton and an electron concentration $x = 10^{-3}$ are: $Q(H_2) \tilde{=} 15$ eV, $Q(H) = 8.0$ eV, and $\phi(H_2) = 1.3$, $\phi(H) = 1.5$. As will be seen from the results given in Section III, cosmic ray heating alone can not produce the observed temperatures of interstellar clouds even with substantial coolant depletion unless unreasonably large values of the cosmic ray ionization $\zeta_p \gtrsim 10^{-15} s^{-1}$ are assumed. We have therefore been led to consider a number of other heating mechanisms

to see whether either singly or together they might not contribute significant heating.

(1) H_2 Dissociative Heating

Stephens and Dalgarno (1973) have suggested that the 2 H atoms from the photo dissociation of H_2 may cause significant heating of the gas. The heating rate may be written as

$$\Gamma_{diss} = \eta\, n(H_2) \left\langle \Delta E_h \right\rangle_{diss} , \qquad (23)$$

where η is the photo-dissociation rate discussed above, and $\left\langle \Delta E_h \right\rangle_{diss}$ is the mean heating per dissociation:

$$\left\langle \Delta E_h \right\rangle_{diss} = \frac{\sum_{v'JJ'} \eta_{OJ,v'J'} \Delta E_{v'}}{\sum_{v'JJ'} \eta_{OJ,v'J'}} \qquad (24)$$

In (24), $\eta_{OJ,v'J'}$ is the rate per H_2 for dissociation via B v'J' ← XOJ and $\Delta E_{v'}$ is the corresponding mean kinetic energy released, calculated by Stephens and Dalgarno (1973). Eq. (23) is based on 100% efficiency for conversion of H-atom kinetic energy into gas heating. For a very diffuse cloud $\left\langle \Delta E_h \right\rangle_{diss} = 0.42$ eV. By using (8) we find for $\eta \gg R_1 n$, i.e. the outer portions of a cloud,

$$\Gamma^{(0)}_{diss} = R_1 n^2 \left\langle \Delta E_h \right\rangle_{diss}$$

$$= 6.72 \times 10^{-30} \text{ ergs cm}^3\text{s}^{-1}\, n^2 \times \left(\frac{R_1}{10^{-17}\text{cm}^3\text{s}^{-1}} \right) \qquad (25)$$

Γ_{diss} will slowly decrease going into the cloud.

(2) Grain Photoelectron Heating

Watson (1972) has advocated reconsideration of grain photoelectric heating (Spitzer, 1948) because the photoelectron yield above 10 eV is now known to be considerably larger for some representative materials than the values used in earlier estimates. This point must still remain uncertain since the surface properties of interstellar grains are unknown. Watson (1974) has also noted that certain ice mantles, which are frequently postulated in grain models, may be inefficient photoelectron producers. On the other hand, irregularities, impurities, and small grain size, all help to increase the efficiency. In any case it now seems appropriate to consider the effects of grain heating on the thermal properties of interstellar clouds.

Following Watson (1972) we adopt an extremely simple formula for grain photoelectron heating in view of the numerous uncertainties in the physical properties of the emission process,

$$\Gamma_{gr\ ph\ el} = \bar{y} \left\langle \Delta E_h \right\rangle_{gr} \int_{912A}^{\lambda_1} d\lambda\, \sigma_{gr\ abs}(\lambda) \left[c_{cont} \pi I(\lambda, x) \right] \qquad \text{.....(26)}$$

The cut-off λ_1 is the wave-length below which the photoelectron yield assumes a relatively constant value according to Watson (1974). Both the yield and the photoelectron energy have been extracted from integrals as the mean values $\bar{y}$ and $\left\langle \Delta E_h \right\rangle_{gr}$. In particular, $\lambda_1 \simeq 1240$ Å, $\left\langle \Delta E_h \right\rangle_{gr} = 1.8$ eV, and very uncertainly

$0.03 < \bar{y} < 0.2$. The quantities in the integral (26) have been discussed above. For a very diffuse cloud without attenuation, we can estimate (26) approximately in terms of a mean grain absorption cross section and a mean radiation field:

$$\Gamma^{(0)}_{\text{gr ph el}} \simeq 1.25 \times 10^{-26} \text{ergs s}^{-1} \cdot n \times (\bar{y} / 0.1)(I/4 \times 10^{-9} (\text{cm}^2 \text{s str H}_z)^{-1})(\sigma_{\text{gr abs}}/10^{-21}\text{cm}^2) \quad \ldots\ldots\ldots(27)$$

Equations (26) and (27) are based on 100% heating efficiency for the heating of electrons with mean energy $\sim$ 2 eV (Glassgold and Langer, 1973b). Possible effects of grain charge have also been ignored since the best estimates of the grain potential energy U (Feuerbacher et al, 1973) indicate that $|U| \ll \langle \Delta E_h \rangle_{gr}$.

(3) H_2 Formation Heating

Spitzer and Cochran (1973) have proposed that newly formed H_2 molecules have considerable internal and translational energy in order to account for the increase in velocity dispersion with rotational quantum number J observed with OAO-3. They have also suggested that the kinetic energy, which they estimate to be $\sim$ 3 eV, can heat the gas. We have included this new heating mechanism in our program as

$$\Gamma_{\text{form}} = R_1 \, n(H) \, n \langle \Delta E_h \rangle_{\text{form}} = 7.16 \times 10^{-29} \text{ ergs cm}^3\text{s}^{-1} (1 - f) \, n^2 \times (\langle \Delta E_h \rangle_{\text{form}} / 4.48 \text{ eV}) (R_1/10^{-17}\text{cm}^3\text{s}^{-1}) . \quad \ldots\ldots\ldots(28)$$

The relative importance of the heating mechanisms investigated here depends sensitively on parameters which are not directly observable and which are also difficult to estimate theoretically. The only one which can be calculated with confidence is H_2 dissociative heating (Stephens and Dalgarno, 1973). Thus we will vary the parameters in each heating mechanism over a fairly large range in order to understand its potential for heating. Finally, for comparison we give the cosmic ray heating for a mixture of H, He, and H_2 (see Appendix B).

$$\Gamma_{CR} \simeq (1 + \xi(He)) \zeta_p(H) n(8 \text{ eV} + f\ 7.6 \text{ eV}) \qquad (29)$$

III. Results

We present our results through a series of figures and accompanying comments. Most of the figures are in the form of fractional H_2 abundance F and neutral C column density $N[CI]$ vs. total hydrogen abundance N, as in Figs. 2-4, 6-10. F is defined as

$$F = 2N[H_2]/N = 2N[H_2]/(N[H] + 2N[H_2]). \qquad (30)$$

In this type of figure, there are always two common curves (one for F and one for $N[CI]$) against which the effects of changing individual model parameters can be gauged. The parameters for this "standard" run are given in Table II. Most of the reaction rate constants are listed in Table A of Appendix A. The parameters in the standard run have not been

determined by any systematic analysis, and we do not expect them to provide quantitative agreement with any particular cloud. On the other hand, this standard run is qualitatively similar to those we might use in attempting to obtain detailed fits to observations for diffuse clouds.

In Fig. 2 we see that changing the Doppler shift parameter b_D has a large effect at small column densities $N < 1 \times 10^{20} cm^{-2}$, but essentially no effect on other constituents such as C. We note that the large variation in F occurs in the range $N = (10^{19} - 10^{20})\ cm^{-2}$, which is where the self-shielding of the dissociating Lyman band line radiation of H_2 molecules takes place. The narrower the lines, i.e. the smaller b_D, the more rapidly (as a function of N) do the Doppler cores of the lines become optically thick and newly formed H_2 molecules protected from being dissociated. Hence the regular increase in F as a decreasing function of b_D in Fig. 2. In the transition region in Fig. 2, the strongest Lyman line has its Doppler core completely absorbed for $N \simeq 10^{19}\ cm^{-2}$, i.e. the optical depth is e for this N at the frequency where the Doppler and radiative line profiles are equal. By the same criterion, essentially all Lyman band line cores are absorbed when $N \simeq 1 \times 10^{20} cm^{-2}$. Beyond $N > 10^{20} cm^{-2}$, the absorption occurs in the radiative wings. In this region the variation in H_2 abundance can be obtained in closed form if line photo-dissociation is the only destruction mechanism (Solomon and Wickramasinghe, 1969; Jura, 1974).

We have compared our calculations of H_2 abundances with those of Hollenbach, Werner, and Salpeter (1971). When account is taken of numerous differences in methods of calculation, e.g. in radiation field, geometry, grain absorption, transition probabilities, etc., satisfactory agreement

is obtained with the results presented in their Figs. 1 and 3. As noted by Spitzer et al (1973), the abundances of H_2 observed with Copernicus are in qualitative agreement with the predictions of Hollenbach et al and thus with the type of curve presented in Fig. 2.

At the surface of a diffuse cloud, (11) applies with a dissociation rate $\eta_0 \gg R_1 n$ unaffected by attenuation, i.e.

$$f_0 = \frac{R_1 n_0}{\eta_0} \quad . \tag{31}$$

For the standard run in Fig. 2 (b_D = 4 km/s), n_0 = 32 cm^{-3}, $\eta_0 = 0.44 \times 10^{-10} s^{-1}$, $R_1 = 3 \times 10^{-17} s^{-1}$, so that $f_0 = 2 \times 10^{-5}$. This value is actually four times the value calculated in our program for N = 0 and plotted in the figures. This is because it is based on the value $c_{line} = 4$, i.e. on the assumption that the surface of a diffuse cloud is fully illuminated by the interstellar radiation field. Large departures from $f_0 = 2 \times 10^{-5}$ can be obtained for different choices of the parameters as we have argued earlier (Glassgold and Langer, 1973c). Jura (1974) has recently discussed the effects of changing η_0 which arise from the proximity of a cloud to a star and from shielding of the dissociating radiation by other clouds.

The effect of varying c_{cont} is given in Fig. 3; $c_{cont} = 4$ corresponds to an optically thin cloud whereas $c_{cont} = 1$ would be appropriate to a very large optical depth. Only the extreme limits of the slight variation with F are given in Fig. 3. The variation of N [CI] is much larger. Recalling the discussion near the end of Sec. II.C, we note that exact solutions suggest $c_{cont} \simeq 2$ for a slab and $c_{cont} \simeq 3$ for a sphere for optical depths to cloud center $\tau_o \simeq 1$. For a given geometry, errors

made by using a constant c_{cont} are typically 10% in N [CI], but may be as large as 25% near the cloud surface.

The effect of varying the pressure p_o is illustrated in Fig. 4. Both F and N [CI] increase with p_o because the density n increases with p_o. The temperature profiles for the four calculations of Fig. 4 are shown in Fig. 5(b). For reasons to be discussed later, the temperature varies only slightly with N for the type of model defined by the parameters in Table 2. The mean temperature also changes little when substantial changes are made in p_o because T is controlled by Boltzmann factors in the cooling transitions in (4), i.e. only small changes in T are needed to accommodate large changes in other quantities in the balance equations. Thus the major effects of changing p_o can be traced to a change in density. The mean temperature is usually given for each calculation as a label located near the F vs. N curve. The density profiles for H and H_2 are plotted in Fig. 5(a). Most of the increase in n is associated with conversion of H to H_2 at constant T. If we set $n(H) + n(H_2) = (1 - \frac{f}{2})\, n = p_o/kT$ and replace T by $\overline{T}$, then the variation in n can be approximately accounted for by

$$n = \frac{p_o/k\overline{T}}{1 - f/2}$$

The curves in Fig. 6 show the effect of varying the cosmic ray flux parameterized by the primary ionization $\zeta_p(H)$ per H atom. The actual ionization rate is increased through the action of the primary and secondary electrons, and depends on the composition of the medium. The rates for H, H_2, and He are listed in Table A, and the effective rate for a mixture of H,

H_2, and He is discussed in Appendix B. The range considered for ζ_p goes from the large value ($10^{-15}s^{-1}$) used a few years ago in the 2-phase model to a value ($10^{-18}s^{-1}$) about a factor of 2 smaller than the extrapolation by Spitzer and Tomasko (1968) from the observed flux above 1 GeV. The main effect of changing ζ_p in Fig. 6 is to change the electron density, in accord with (17). This is the reason for the large changes in $N[CI]$, as dictated by the C balance based on (12). The mean electron densities are included as an extra label on the $N[CI]$ curves in Fig. 6. Another aspect of Fig. 6 is that the temperature is altered because a significant part of the cooling comes from electron collisions with C^+ ions. This then has an effect on the density through the gas law (3), and consequently on the H_2 abundance. When ζ_p approaches $10^{-15}s^{-1}$, another factor enters into the determination of T, heating by the cosmic rays. The mean temperature for $\zeta_p = 10^{-15}s^{-1}$ actually increases relative to the standard run, despite the enhanced cooling arising from the factor of 4 increase in n_e. In this case cosmic ray heating becomes the largest of the heating mechanisms, i.e. $\Gamma_{CR} \simeq (0.5 - 0.7)\,\Gamma_{tot}$.

Another aspect of the $\zeta_p = 10^{-15}s^{-1}$ curve in Fig. 6 is the large reduction in H_2 abundance for $N > 2 \times 10^{20}cm^{-2}$, which occurs because cosmic ray ionization of H_2 has become the major mechanism for H_2 destruction. Table III presents the total column density at which cosmic ray destruction is 1/2 the photo destruction rate. For the smaller values of $\zeta_p \lesssim 10^{-16}s^{-1}$, cosmic ray destruction is not very important for $N < 10^{21}$ cm so that the H_2 abundance ratio F can not provide much more than a very rough upper limit to ζ_p. Furthermore, F is sensitively affected by other as yet undetermined parameters such as the UV field I and the formation rate R_1 (see Figs. 8 and 9). Perhaps the most important

conclusion here is that the abundance of atomic H at large column densities $N \gtrsim 10^{21} cm^{-2}$ is influenced by cosmic rays, as suggested by Solomon and Werner (1971). It must be realized, however, that a quantitative evaluation of n(H), i.e. to better than a factor of 2, is impossible unless the branching between the dissociative recombination channels for H_3^+ (3H vs. H_2 + H) is known.

In Fig. 7 the effect of changing the depletion of C is portrayed. Besides the direct obvious increase of N [CI] with the relative abundance $\xi(C)$, increasing $\xi(C)$ lowers the temperature by increasing the cooling rate. This then increases the density, which generally promotes the formation of H_2, and explains the upward shifting of the F curves with $\xi(C)$. The increase in density further amplifies the abundance of CI since both the total C density and the electron density are increased. The curve for the solar abundance $\xi(C) = 4 \times 10^{-4}$ seems to be well above the preliminary Copernicus determinations of N [CI] (Morton et al, 1973). The temperature is also significantly lower in this case than for depletion factors in the range from 4-8.

The curves in Fig. 8 exhibit the effect of changing the radiation field. The labels I_1 - I_4 refer to the four radiation fields given in Fig. 1 and discussed in Section II. The main trend of the curves can again be understood qualitatively in terms of the thermal balance appropriate to each field, when we recall that the sequence I_1, I_2, I_3, I_4 correspond to increasing values for the total integrated UV flux. Since the main heating mechanisms in the model are proportional to the flux, the temperatures increase and the densities decrease as we go through this sequence. The calculated changes in densities are actually larger, however, because of

the varying degrees of conversion to molecular hydrogen. The four radiation fields have different shapes, and their relative abilities for H_2 dissociation are different than for heating. (The fluxes at 1000 Å are $\sim$ 1.5, 2.4, 4.0, and 5.0 x 10^{-8} photons/cm^2s Hz^{-1} for the four fields I_1, I_2, I_3, and I_4, respectively.) Furthermore, the relationship between dissociating intensity and gas density is non-linear, so that it is difficult to sort out the causes of the changes in these curves.

Some effects of varying the rate constant R_1 for H_2 formation on grains are shown in Fig. 9. The variation in R_1 by a factor of 50 leads to the very large variations depicted for F, but the differences tend to be compressed once $N \gtrsim 10^{20} cm^{-2}$. The spreading apart of the N[CI] curves with increasing N arises in a complicated way from several factors which lead to small decreases in n_e and n(CII) with increasing R_1. These changes arise from an increase in temperature associated with a significant reduction in CII cooling via excitation by H atoms. For example, n(H) at N = 5 x 10^{20} decreases from $\sim$ 30 cm^{-3} for R_1 = 5 x $10^{-18} cm^3 s^{-1}$ to $\sim$ 4 cm^{-3} for $R_1 = 10^{-16} cm^3 s^{-1}$. We are assuming that H_2 collisions are ineffective in exciting CII (Glassgold and Langer, 1973a).

In the above figures we have attempted to show the effects of changing individual model parameters. These changes can be very substantial, but changes in one parameter can often be compensated by changes in another, and this will surely make it difficult to obtain a unique set of parameters. In Fig. 10, the pressure and the radiation field have been simultaneously increased by factors of 2 and of 5 in the two sets of solid curves. The change in radiation field is achieved by simple scaling of the Habing

field I_2. Increases by these amounts might arise from the proximity of a cloud to a hot star (Herbig, 1968; Jura, 1974). The exact amount will depend on distance, and one side of the cloud will be illuminated more than the other--an effect not included in the present calculations. The curves in Fig. 10 have been plotted on an expanded scale to illustrate how little the relative H_2 abundance F is changed. This result is not too surprising in view of the fact, already noted in connection with Fig. 4, that the main effect of varying p_o is to change the density. According to (11), the fractional abundance is determined by the ratio of UV dissociation rate to density, and in Fig. 10 this ratio is nearly constant. The relatively small increases in temperature have a complicated explanation in the changes in the n-dependence of the heating and cooling rates and in the relative importance of e and H excitation of CII. The electron density follows (17) and, consistent with (12) for n(CII) >> n(CI), leads to the decreases in Fig. 10 which are roughly proportional to $\sqrt{2}$ and $\sqrt{5}$.

Model calculations for large p_o and $\bar{n}$ are of interest in connection with the high densities $\sim 10^3 cm^{-3}$ suggested for the ζ Oph cloud by Herbig (1968) and by Black and Dalgarno (1973b). The latter authors have suggested that increasing the radiation field and the density may account for the observed H_2 rotational state populations (Spitzer and Cochran, 1973) in the context of a collisional-radiative steady state. Although the same range of H_2 fractional abundance F can be achieved, such models imply substantial changes in other constituent densities. Moreover, the very large kinetic pressures required ($10^4 - 10^5$ ^oK cm^{-3}) require

reconsideration of the stability of such cloud masses.

The temperature profiles for the standard parameter set of Table II were given in Fig. 5(b) along with those for different pressures. The standard run yields a mean temperature of $\overline{T} \sim 63^{\circ}$ K, which is somewhat lower than the $\sim 80^{\circ}$ K deduced by Spitzer and Cochran (1973) for OAO-3 clouds. When we reexamine the $\overline{T}$ labels in Figs. 4-10, however, we see that many of the parameters affect the temperature so that only relatively slight adjustments would be required to boost $\overline{T}$ to 80° K. In addition to varying p_o, ζ, I_1, R_1, and especially $\xi(C)$, we can also vary somewhat the strength of the heating mechanisms.

The temperature profiles in Fig. 5(b) are fairly typical of our model calculations for diffuse clouds. Deviations from $\overline{T}$ tend to be $< 10\%$ for $N < 10^{21} cm^{-2}$. The approximate isothermality stems from the near constancy of the important heating rates in Eqs. (25) - (29). The component heating rates are shown in Fig. 11(a) for the standard run and in Fig. 11(b) for the case in which the photoelectron efficiency has been increased to $\overline{y} = 0.2$ ($\overline{T} = 80^{\circ}$ K in this case). Dissociative heating accounts for only a few percent of the heating and has been omitted from the figures. Cosmic ray heating is minor but not negligible when $\zeta_p(H) = 10^{-16} s^{-1}$, but it would become negligible if ζ_p were reduced to $10^{-17} s^{-1}$ or less. In the standard run, grain photoelectron heating and H_2 formation heating are comparable, accounting on the average for 45% and 40% of the heating, respectively. If we had to rely on just one of these two heating mechanisms, then $\overline{T}$ would drop to $\sim 40^{\circ}$ K if no other changes were made. But we might then also consider increasing the strength of the single source as well as making slight changes in

parameters such as p_o, I, R, and $\xi(C)$. However, we would be hard pressed to achieve $\overline{T} = 80^\circ$ K with just formation heating because the mean heating $\langle \Delta E_h \rangle_{form}$ associated with a newly formed H_2 molecule is limited by observations (Spitzer and Cochran, 1973). In the standard run, we already used two-thirds of the maximum allowed value of 4.5 eV, and it is really difficult to comprehend unit efficiency in this process. Grain photoelectron heating seems more promising to us in that efficiencies $\overline{y}$ in the 10-20% range can provide $\overline{T}$ of 80-100° K. Thus $\overline{T} = 80^\circ$ K for the calculation in Fig. 11(b), where the only change from Table II is $\overline{y} = 0.2$. To illustrate the effect of several rather not unreasonable changes, we found that when p = 1500, $\zeta = 5 \times 10^{-17} s^{-1}$, $\xi(C) = 5 \times 10^{-5}$, $R_1 = 5 \times 10^{-17} cm^3 s^{-1}$, T reached 140° K and 105° K, at the surface and interior, respectively, for an average of $\overline{T} \approx 110^\circ$ K. Of course the other effects of such changes would have to be confronted with relevant observations before drawing any conclusion other than that a fair range of temperature is possible in this model.

We have also applied our model to the Ca ionization equilibrium, making specific use of (12), (13), and Table I. Our calculations differ from earlier ones (e.g. Herbig, 1968; Brown, 1972; Pottasch, 1972; White, 1973) in that our photoionization rate is at least a factor of 2 larger, reflecting more recent cross section measurements (Carter et al, 1971; McIlrath and Sandeman, 1972). In addition, our model is generally more complete; it includes, for example, inhomogeneous electron and hydrogen densities. The calculated density ratios n(CaII)/n(CaI) decrease typically by a factor of 2 when N varies from 0 to 8×10^{20} cm^{-2}. This is somewhat less than expected solely on the basis of radiation transfer considerations, and reflects the effects of decreasing electron density

and CaIII density going into the cloud. Density inhomogeneities do not cause appreciable differences between $N[CaII]/N[CaI]$ and $n(CaII)/n(CaI)$ until $N > 5 \times 10^{20}$ cm, where they are $\sim$ 10%.

Our calculated $N[CaII]/N[CaI]$ ratios are typically of order of magnitude 10^3, whereas the values deduced from interstellar absorption lines (Pottasch, 1972; White, 1973) are closer to 10^2. Using a sensitive synthesis technique, Bortolot, Shulman, and Thaddeus (1974) have reported a ratio very close to 100 for ζ Oph. Although the calculated ratios can be reduced somewhat, it is hard to obtain a factor of 10 reduction without running into other difficulties, such as low temperatures or requiring high cosmic ray fluxes, weaker UV fields than Habing's, and C abundances near solar.

Another way of describing this situation is that the electron densities deduced from measured CaI and CaII interstellar absorption lines are about a factor of 5 to 10 larger than given by our model. The values suggested seem to be $\gtrsim$ 0.1 cm^{-3} (e.g. White, 1973). These determinations are based on a single cloud component picture in which the various factors in the ionization balance equation (12) are replaced by mean values, and densities by column densities. Such a simplified picture may not be appropriate, however, and important contributions to the relevant column densities may come from the intercloud medium and/or the immediate neighborhood of the star. For example, the recombination coefficient for CaII may be at least as big in a hot intercloud medium (as in a cool cloud) because of dielectronic recombination (Pottasch, 1972). If the electron densities are about the same in the intercloud and cloud phases, as is often stated (see the review by Dalgarno and McCray, 1972), then the intercloud region may play an

important role in the analysis of CaII to CaI column density determinations.

The Copernicus observations (Morton et al, 1973) only determine N[CII] to within an order of magnitude for the four stars, ξ Per, α Cam, ζ Oph, and γ Ara. Since most of the gas-phase C is in CII, these measurements correspond to depletion relative to the solar abundance by a factor in the range from 2 to 20. The measurements of N [CI] are more precise, and the average for five stars (the above mentioned plus λ OriA) seems to be about $\sim 3 \times 10^{-7}$ N. The values of N [CI] obtained from our standard run seem to be somewhat smaller by a factor of $\sim 1\frac{1}{2}$ to 2. We do not believe that this difference should be taken too seriously, since the standard parameters were rather arbitrarily selected. The calculated values of N [CI] are quite sensitive to the choices in certain parameters as shown in the above figures. Larger values for N [CI] could be obtained, for example, by reducing c_{cont}, I, and R_1, or by increasing p_o, $\xi(C)$, and ζ_p. These effects can be understood in terms of the basic balance equation (12), which we rewrite for C with the approximation $n(CI)/n(CII) = n_e\alpha(CII)/G(CI) << 1$, as

$$n(CI) \simeq \frac{n_e \alpha(CII)}{G(CI)} \xi(C)\, n \qquad (32)$$

Additional simplifications would usually be made in applying (32) to measured column densities, which could cause substantial errors. For example, N [CI] /N will become substantially smaller than n(CI)/n for $N > 3 \times 10^{20} cm^{-2}$ simply because of density inhomogeneities. With caution we can interpret the OAO-3 observations to imply an average $n(CI)/n \sim 3 \times 10^{-7}$ and then use (32) to estimate $n_e \xi / G_o(CI) \sim 2.6 \times 10^4 cm^3 s^{-1}$, where $G_o(CI)$ is the CI photoionization rate at the surface of a diffuse

cloud. In other words, in this interpretation the present measured values of $N[CI]$ determine only the product of three relatively poorly known quantities. If we use Jura's field ($G_o \sim 2.5 \times 10^{-10} s^{-1}$), then $n_e \sim 0.03$ cm^{-3} and ~ 0.003 cm^{-3} for $\xi(C) = 2 \times 10^{-4}$ and 2×10^{-5}, respectively, corresponding to depletion factors of 2 and 20. Although this argument is very crude, it suggests that our model calculations may be able to explain the OAO-3 CI measurements with fairly small electron densities and cosmic ray ionization rates $\zeta_p(H) < 10^{-16} s^{-1}$. This situation is almost the reverse of that discussed above for Ca. The Ca observations have been interpreted by White (1973) to imply electron densities much larger than are obtainable with the "intermediate" cosmic ray ionization rate $\zeta_p(H) = 10^{-16} s^{-1}$. Our own preliminary qualitative conclusion from the OAO-3 CI data is that $\zeta_p(H) \lesssim 10^{-16} s^{-1}$, consistent with the crude upper limit deduced from relative H_2 abundances F in the thicker OAO-3 clouds. The same conclusion has been reached by Black and Dalgarno (1973a), Jura (1974), and O'Donnell and Watson (1974) by consideration of the HD column densities measured by Spitzer et al (1973). These authors obtain values for ζ_p which generally lie in the range $10^{-17} s^{-1} - 10^{-16} s^{-1}$.

IV. Conclusion

The results presented in Section III suggest that the model defined in Section II may be useful in interpreting interstellar absorption lines arising from diffuse clouds. Although detailed analyses of individual clouds must still be carried out, the model does seem to be capable of reproducing the general trend of H_2 fractional abundances and kinetic

temperatures observed by OAO-3. More quantitative tests of the model should be carried out as more extensive data becomes available, e.g. of the type recently reported by Spitzer, Cochran, and Hirshfeld (1974) for H_2. Many applications, improvements, and extensions of this model are suggested by our preliminary discussion in Section III. We are currently engaged in a more complete investigation of the roles of other molecules which would be applicable to both OAO-3 clouds and to thicker ones.

This work has been supported by Grant NGR-33-016-196 from the National Aeronautics and Space Administration.

Appendix A. Ionization Balance

The reactions required for treating the electrical balance equation (5) are listed in Table A. Our treatment is restricted to molecular hydrogen clouds in which the ionization of C is still dominated by the interstellar UV field, i.e. $N < 10^{21} cm^{-2}$. Oppenheimer and Dalgarno (1974) have recently considered the ionization of denser interstellar clouds. Previous treatments of this problem under more simple conditions have been given by Werner (1970), Solomon and Werner (1971) and de Jong (1972). The total rate for A6 is much larger than was given by Solomon and Werner since they ignored electronic dissociation of H_2 (Glassgold and Langer, 1973b).

The balance equations arising from the reactions in Table A are:

$$H_2: \quad R_1 n(H) n + K_1 n(H) n(H_2^+) + \beta_3 (H_2 + H) n_e n(H_3^+) = (\zeta_2 + \eta) n(H_2) + K_2 n(H_2) n(H_2^+) \quad (A17)$$

$$H_2^+: \quad \zeta_2(H_2^+) n(H_2) = n(H_2^+) \left[K_1 n(H) + K_2 n(H_2) + \beta_2 n_e \right] \quad (A18)$$

$$H_3^+: \quad K_2 n(H_2) n(H_2^+) = \beta_3 n_e n(H_3^+) \quad (A19)$$

$$H^+: \quad \zeta_1 n(H) + \zeta_2(H^+) n(H_2) + K_1 n(H_2^+) n(H) = \alpha(H^+) n_e n(H^+) \quad (A20)$$

$$He^+: \quad \zeta(He) n(HeI) = \alpha(He^+) n_e n(HeII) \quad (A21)$$

$$C^+: \quad G(CI)\, n(CI) = \alpha(C^+) n_e n(CII) \quad (A22)$$

with

$$\zeta_2 = \zeta_2(H_2^+) + \zeta_2(H^+) + \zeta_2(2H) \quad (A23)$$

$$\beta_3 = \beta_3(H_2 + H) + \beta_3(3H) \quad (A24)$$

In addition, the total densities for H, He, and C are:

$$n = n(H) + n(H^+) + 2n(H_2) + 2n(H_2^+) + 3n(H_3^+) \quad (A25)$$

$$n(He) = n(HeI) + n(HeII) = \xi(He) n \quad (A26)$$

$$n(C) = n(CI) + n(CII) = \xi(C)n \tag{A27}$$

and

$$n_e = n(H^+) + n(H_2^+) + n(H_3^+) + n(HeII) + n(CII) \tag{A28}$$

The effects of the charge exchange reactions (Field and Steigman, 1972)

$$O^+ + H \rightleftarrows O + H^+ + 0.002 \text{ eV}$$

have not been included in the above balance equations. The potential importance of these reactions for $n(H^+)$ and n_e has been emphasized by Watson (1973), Dalgarno, Oppenheimer, and Berry (1973), and Black and Dalgarno (1973), especially for dense clouds. We have included these reactions in a more elaborate theory of ionization than presented here, and find that O - H charge exchange is not important in determining the electron density in the relatively thin, low density clouds under consideration in this paper. Our quantitative estimates invoke significant depletion of O (by at least a factor of 5) suggested by OAO-3 observations (Morton et al, 1973) and the strong temperature dependence of the $O + H^+ \rightarrow O^+ + H$ rate. The physical reason why O charge exchange is not important for diffuse clouds is that they still have sufficient atomic H for the exothermic exchange $O^+ + H \rightarrow O + H^+$ to compete favorably with H_2 - induced formation of rapidly recombining molecular ions such as OH^+, H_2O^+, etc.

In order to express all of the densities in terms of n and the various rate constants in a relatively simple way, we make the approximation of ignoring $\beta_2 n_e$ in (A18), that is we ignore dissociative recombination (A12) as a destruction mechanism for H_2^+ compared to charge exchange with H_2 (A15) and the H_3^+-producing ion-molecule reaction (A16). This approximation

requires low electron density, i.e.:

$$x_e << x_1 \equiv \frac{K_1 + (K_2/2 - K_1)f}{\beta_2} \tag{A29}$$

With the rate estimates of Table A and T = 100° K, $x_1 = 0.1\ (1 + 2/3\ f)$, i.e. the condition (A29) would be easily satisfied for interstellar clouds. This estimate is based on theoretical estimates for K_1 and β_2. The latter is $\sim 10^2$ smaller than many measured dissociative recombination rates for other species. However, we expect our approximation to be accurate even if x_1 is as large as 10^{-3}.

With this approximation, the above system (A17)-(A28) can be solved as follows. First, the densities for H_2^+, H_3^+, and H_2 can be obtained in terms of n and n_e:

$$n(H_3^+)/n(H_2^+) = (K_2/2\ \beta_3)(f/x) \tag{A30}$$

$$n(H_2^+) = 1/2\ \zeta_2(H_2^+)\ f\ \left[K_1 + (K_2/2 - K_1)f\right]^{-1} \tag{A31}$$

$$f = 1/2\ \ (-b + \sqrt{b^2 - 4ac}\ )/a \tag{A32}$$

with

$$a = (2R_1 n)(K_2/2\ \ - K_1) + (K_1 + K_2/2\ \ \beta_3(3H)/\beta_3)\ \zeta_2(H_2^+) \tag{A33}$$

$$b = \zeta_2 + \eta - K_1\zeta_2(H_2^+) + (2R_1 n)(2K_1 - K_2/2) \tag{A34}$$

$$c = (2R_1 n)K_1 \tag{A35}$$

Eqs. (A30) and (A31) imply that the densities of the hydrogen molecular ions are negligible, e.g. when $\zeta_2(H_2^+) \sim 3 \times 10^{-16} s^{-1}$, $n(H_2^+) < f\ 10^{-6} cm^{-3}$ and $n(H_3^+) < f^2\ 5 \times 10^{-6}\ cm^{-3}$. Then (A28) becomes

$$n_e = n(H^+) + n(HeII) + n(CII) \tag{A36}$$

Where the individual densities are given by

$$n(H^+) = \frac{\zeta_H\, n}{\alpha(H^+) n_e} \tag{A37}$$

$$n(HeII) = \frac{\zeta(He)\ \xi(He) n}{\alpha(He^+)\ n_e} \tag{A38}$$

$$n(CII) = \frac{G(CI)\ \xi(C) n}{\alpha(C^+)\ n_e}\ \left(1 + \frac{G(CI)}{\alpha(C^+) n_e}\right)^{-1} \tag{A39}$$

and ζ_H is an effective ionization rate for hydrogen,

$$\zeta_H = \left\{\zeta_1 + 1/2\ \zeta_2(H_2^+)\ \left[\frac{K_1 f}{K_1 + (K_2/2 - K_1)f}\right]\right\}(1-f) + 1/2\ \zeta_2(H^+) f \quad . \tag{A40}$$

We have assumed that $n(HeII) < < n(HeI)$. When (A37)-(A39) are put into (A36), a cubic equation results; we have solved the system (A35)-(A40) by iteration.

When $n(CII) > > n(CI)$, the equation for n_e reduces to the quadratic

$$n_e^{\,2} - \xi(C) n\ n_e - \frac{\zeta' n}{\alpha(H^+)} = 0 \quad , \tag{A41}$$

where ζ' is defined as

$$\zeta' = \zeta_H + \frac{\alpha(H^+)}{\alpha(He^+)}\ \xi(He)\ \zeta(He) \ . \tag{A42}$$

If we assume that all atoms with ionization potentials < 13.6 eV are predominantly doubly ionized, then $\xi(C)$ in (A41) is replaced by the total abundance ξ_{HA} of these heavy atoms, and (A40) has the solution

$$x_e = 1/2\ \left[\xi_{HA} + \sqrt{\xi_{HA}^2 + 4\ \zeta'/n\alpha(H^+)}\right]. \tag{A43}$$

This is a generalization of earlier results (e.g. Preston and Brown, 1970) to include H_2 and He.

Appendix B. Cosmic Ray Heating of H_2, H, He Mixtures

The heating of a gas of H_2 molecules by cosmic rays has been studied by Glassgold and Langer (1973b). Regions containing only atomic H had been studied earlier by a number of authors, e.g. Goldsmith, Habing, and Field (1969) (see Glassgold and Langer, 1973b, for other references). In this appendix we give an approximate treatment for a mixture of H, H_2, and He, appropriate to the central parts of diffuse OAO-3 clouds. We also discuss the dissociation rate $\zeta_2(2H)$.

We estimate the heating by following the evolution of the electrons produced by ionization of H, H_2, and He by cosmic rays, following closely our earlier work. The ionization of H and H_2 yields a primary electron with a mean energy $\simeq$ 20 eV. The H_2^+ ion leads to a characteristic chemical heating, $Q_{ion}(He) \simeq 7$ eV, which arises from reactions (16.b) and (16.c). The associated heating rate is

$$\Gamma_{ion}(H_2) = Q_{ion}(H_2)\, \zeta_p(H_2^+)\, n(H_2) \quad , \tag{B1}$$

where $\zeta_p(H_2^+)$ is the primary ionization rate for the reaction (A4). The mean primary ionization rate, $\zeta_p(e^-)$, is given by

$$\zeta_p(e^-) = \tfrac{1}{2} f\, \zeta_p(H_2^+) + (1 - f)\, \zeta_p(H) + \xi(He)\, \zeta_p(He) \quad , \tag{B2}$$

where $\xi(He)$ is the fractional abundance of He. The primary electrons coming from ionization of H, H_2, and He may follow any one of these channels:

$$\begin{aligned} e + H_2 &\rightarrow H_2^+ + e_1 + e_2, && E_1(e) + E_2(e) = 5 \text{ eV}, && \sigma = 4 \times 10^{-17} \text{cm}^2 \\ &\rightarrow H_2^* + e_1, && E_1(e) = 9 \text{ eV}, && \sigma = 4 \times 10^{-17} \text{cm}^2 \\ &\rightarrow H + H + e, && E_1(e) = 8 \text{ eV}, && \sigma = 6 \times 10^{-17} \text{cm}^2 \end{aligned} \tag{B3}$$

$$e + H \rightarrow H^+ + e_1 + e_2 , \quad E_1(e) + E_2(e) = 7 \text{ eV}, \quad \sigma = 3 \times 10^{-17} \text{cm}^2$$
$$\rightarrow H^* + e_1, \quad E_1(e) = 9 \text{ eV}, \quad \sigma = 4 \times 10^{-17} \text{cm}^2 \qquad (B4)$$

where E(e) gives the mean energy of an outgoing electron, and σ is a typical mean cross-section. The mean secondary ionization rate is given by

$$\zeta_{sec}(e^-) = \left\{ \frac{\sigma_i(H_2)n(H_2) + \sigma_i(H)n(H)}{\sigma_t(H_2)n(H_2) + \sigma_t(H)n(H)} \right\} \zeta_p(e^-) \qquad (B5)$$

where $\sigma_i(x)$ is the ionization and $\sigma_t(x)$ the total cross-section for species X.

The heating due to these secondary electrons is given by

$$\Gamma_{sec} = \zeta_p(e^-)\, n \, \frac{\Sigma\, \sigma_k n(x_k) Q_k(E)}{\Sigma\, \sigma_k n(x_k)} \qquad (B6)$$

where $Q_k(E)$ is the heating for electrons with energy E in channel k. When $x_e \gtrsim 10^{-4}$ we find the following (approximate) form to hold

$$\Gamma_{sec} \simeq \zeta_p(e^-)\, (14\, n(H_2) + 8\, n(H)\,) \text{ eV} \qquad (B7)$$

and that the total heating Γ is given by

$$\Gamma_{CR} \simeq (1 + \xi(He)\,)\, \zeta_p(H)\, n(8 + 7.6\, f) \text{ eV} \quad . \qquad (B8)$$

The total dissociation rate in a mixture can be calculated in a similar manner, yielding

$$\zeta_2(2H) \simeq (0.55 - 0.1\, f)\, \zeta_2(H_2^+) \quad . \qquad (B9)$$

We have neglected the slight dependence on composition and used a mean value of 0.5 $\zeta_2(H_2^+)$ in Table A.

REFERENCES

Adamcyzk, B., Boerboom, A. J. H., Schram, B. L., and Kistenmaker, J., 1966, J. Chem. Phys. 44, 4640.

Allison, A. C. and Dalgarno, A., 1969, JQSRT 9, 1543.

Black, J. H. and Dalgarno, A., 1973a, Ap. J. (Letters), 184, L101.

Black, J. H. and Dalgarno, A., 1973b, Bull. A.A.S. 5, 380.

Bless, R. C. and Savage, B. D., 1972, Ap. J. 171, 293.

Bortolot, V., Shulman, S., and Thaddeus, P., 1974, Ap. J. (submitted).

Bowers, M. J., Elleman, D. D., and King, J., 1969, J. Chem. Phys. 50, 4787.

Brown, R. L., 1972, Ap. J. 173, 593.

Cameron, A. G. W., 1973, "Explosive Nucleo-Synthesis", Ed. D. N. Schramm and W. D. Arnett (Univ. of Texas Press).

Carter, V. L., Hudson, R. D., and Breig, E. L., 1971, Phys. Rev. A4, 821.

Dalgarno, A. and McCray, R. A., 1972, Ann. Rev. Astron. and Astrophys. 10, 375.

Dalgarno, A. and Wright, E. L., 1973, Ap. J. (Letters) 174, L49.

Dalgarno, A., Oppenheimer, M., and Berry, R. S., 1973, Ap. J. (Letters) 181, 95.

Dalgarno, A. and Stephens, T. L., 1972, JQSRT 12, 569.

Dubrovskii, G. V. and Ob'edkov, V. D., 1967, Soviet Astro. AJ 11, 305.

Feuerbacher, B., Willis, R. F., and Fitton, B., 1973, Ap. J. 181, 101.

Field, G. B., Somerville, W. B., and Dressler, K., 1966, Ann. Rev. Astr. and Ap. 4, 226.

Field, G. B., Goldsmith, D. W., and Habing, H. J., 1969, Ap. J. (Letters) 155, L149.

Field, G. B. and Steigman, G., 1972, Ap. J. 166, 59.

Glassgold, A. E. and Langer, W. D., 1973a, Ap. J. (Letters) 179, L147.

Glassgold, A. E. and Langer, W. D., 1973b, Ap. J. 186, 859.

Glassgold, A. E. and Langer, W. D., 1973c, Astrophys. Letters 15,

Goldsmith, D. W., Field, G. B., and Habing, H. J., 1969, Ap. J. 158, 173.

Habing, H. J., 1968, B.A.N. 19, 421.

Herbig, G. H., 1968, Zs. f. Ap. 68, 243.

Herbst, E. and Klemperer, W., 1973, Ap. J. 185, 505.

Hollenbach, D. J. and Salpeter, E. E., 1971, Ap. J. 163, 155.

Hollenbach, D. J., Werner, M. W., and Salpeter, E. E., 1971, Ap. J. 163, 165.

Hughes, M. P., Thompson, A. R., and Colvin, R. S., 1971, Ap. J. Suppl. 23, 323, No. 200.

Jenkins, E. B., Drake, J. F., Morton, D. C., Rogerson, J. B., Spitzer, L., and York, D. G., 1973, Ap. J. (Letters) 181, L122.

de Jong, T., 1972, Astron. and Astrophys. 20, 263.

Jura, M., 1974, Ap. J. (submitted).

Leu, M. T., Biondi, M. A., and Johnsen, R., 1973, Phys. Rev. A8, 413.

Lillie, C. F. (1968), unpublished. Quoted in Witt and Johnson (1973).

Meszaros, P., 1972, Ap. J. 177, 79.

McCrea, W. H. and McNally, D., 1960, M.N.R.A.S. 121, 238.

McIlrath, T. J. and Sandeman, R. J., 1972, J. Phys. B5, L217.

Morton, D. C., Drake, J. F., Jenkins, E. B., Rogerson, J. B., Spitzer, L. and York, D. G., 1973, Ap. J. (Letters) 181, L103.

Neynaber, R. H. and Trujillo, S. M., 1968, Phys. Rev. 167, 63.

O'Donnell, E. J. and Watson, Wm. D., 1974, Ap. J. (submitted).

Oppenheimer, M. and Dalgarno, A., 1974, Ap. J. (submitted).

Penston, M. V., 1970, Ap. J. 162, 771.

Penston, M. V. and Brown, F. E., 1971, MNRAS 150, 373.

Pottasch, S. R., 1972, Astron. and Astrophys. 17, 128.

Radhakrishnan, V., Murray, J. D., Lockhart, P. and Whittle, R. P. S., 1972, Ap. J. Suppl. 24, 15, No. 203.

Seaton, M. J., 1951, MNRAS 111, 368.

Solomon, P. and Werner, M. W., 1971, Ap. J. 165, 41.

Solomon, P. and Wickramasinghe, N. C., 1969, Ap. J. 158, 449.

Spitzer, L., 1948, Ap. J. 107, 6.

Spitzer, L., 1968, Diffuse Matter in Space (Interscience).

Spitzer, L. and Cochran, W. D., 1973, Ap. J. (Letters) 182, L23.

Spitzer, L., Cochran, W. D., and Hirshfeld, A., 1974 (preprint).

Spitzer, L., Drake, J. F., Jenkins, E. B., Morton, D. C., Rogerson, J.B., York, D. G., 1973, Ap. J. (Letters) 181, L116.

Spitzer, L., and Tomasko, M. G., 1968, Ap. J. 152, 971.

Stephens, T. L. and Dalgarno, A., 1973, Ap. J. 186, 165.

Watson, W. D., 1974, "Interstellar Dust and Related Topics", Ed. J. M. Greenberg and H. Van de Holst (Reidel).

Watson, W. D., 1972, Ap. J. 176, 103 and 271.

Watson, W. D., 1973, Ap. J. (Letters) 183, L17.

Werner, M. W., 1970, Astrophys. Letters 6, 81.

White, R. E., 1973, Ap. J. 183, 81.

Witt, A. N. and Johnson, M. W., 1973, Ap. J. 181, 363.

Witt, A. N. and Lillie, C. F., 1973, (preprint).

York, D. G., Drake, J. F., Jenkins, E. B., Morton, D. C., Rogerson, J. B., and Spitzer, L., 1973, Ap. J. (Letters) 182, L1.

Table I.

PARAMETERS FOR THE CHEMICAL EQUILIBRIUM OF C AND Ca

Parameter	Units	CI	CaI	CaII
α (100°K)	$10^{-12}cm^3s^{-1}$	7	7	33
λ_{th}	Å	1101	2028	1044
λ_{th} - 912 Å	Å	189	1116	132
σ_{th}	$10^{-18}cm^2$	11	3.25†	0.167
G/α*	-	20	35	.05

† Average of measured values (Carter et al, 1971; McIlrath and Sandeman, 1972).

* For the case of Habing's radiation field (1968), represented by the average flux for the 1000-2000 Å band as 6.8×10^4 photons/cm^2s Å.

Table II.

PARAMETERS FOR THE STANDARD RUN*

Parameter	Symbol	Value
Pressure	p_o	2000 cm^{-3} k^oK
Cosmic ray ionization rate (primary for H)	$\zeta_p(H)$	$10^{-16} s^{-1}$
Interstellar UV field	I	I_2 - curve 2 in Fig. 1(b)
C abundance	$\xi(C)$	7×10^{-5}
Doppler shift parameter	b_D	4 km s^{-1}
H_2 formation rate constant (on grains)	R_1	$3 \times 10^{-17} cm^3 s^{-1}$
Grain total cross section	$\xi_{gr}\sigma_{gr}(\lambda)$	curve for typical star in Fig. 2(a)
Radiation transfer re-normalization factors	c_{line}	1
	c_{cont}	3
Grain photoelectron efficiency	$\bar{y}$	0.1
Mean formation heating	$\langle \Delta E_h \rangle_{form}$	3 eV

* Reaction rate constants are given mainly in Table A of Appendix A.

Table III

COLUMN DENSITY AT WHICH $\zeta_2(H_2) = 2\eta(H_2, I)$

$\zeta_p(H)$ (s^{-1})	N $(10^{20} cm^{-2})$
10^{-15}	1.9
10^{-16}	10
10^{-17}	23
10^{-18}	38

Table A.

IONIZATION BALANCE REACTIONS

Reaction	Rate	Reference
Grain formation of H_2		
(A1) $H + H \rightarrow H_2$	R_1	Sec. II.B of text and Table II
Photodissociation of H_2		
(A2) $h\nu + H_2 \rightarrow 2H$	η	Sec. II.C of text
Cosmic ray ionization, etc.†		1
(A3) $p + H \rightarrow H^+ + e + p$	$\zeta_1 = 1.5\ \zeta_p$	
(A4) $p + H_2 \rightarrow H_2^+ + e + p$	$\zeta_2(H_2^+) = 2.3\ \zeta_p$	
(A5) $p + H_2 \rightarrow H + H^+ + e + p$	$\zeta_2(H^+) = 0.02\ \zeta_2(H_2^+)$	
(A6.a) $p + H_2 \rightarrow H + H + p$		
(A6.b) $e + H_2 \rightarrow H + H + e$	$\zeta_2(2H) = 0.5\ \zeta_2(H_2^+)$	
(A7) $p + He \rightarrow He^+ + e + p$	$\zeta(He) = 1.5\ \zeta_p$	
Photo ionization		
(A8) $h\nu + C \rightarrow C^+ + e$	G(CI)	Sec. II.B of text
Radiative recombination		2
(A9) $e + H^+ \rightarrow H + h\nu$	$\alpha(H^+) = 2 \times 10^{-10} T^{-0.7} cm^3 s^{-1}$	
(A10) $e + He^+ \rightarrow He + h\nu$	$\alpha(He^+) = \alpha(H^+)$	
(A11) $e + C^+ \rightarrow C + h\nu$	$\alpha(C) = 2 \times 10^{-10} T^{-0.7} cm^3 s^{-1}$	
Dissociative recombination		
(A12) $e + H_2^+ \rightarrow 2H$	$\beta_2 = (4\text{-}8) T^{-\frac{1}{2}} \times 10^{-8} cm^3/s$	3*
(A13) $e + H_3^+ \rightarrow H_2 + H$	$\beta_3(H_2 + H)$	
(A14) $e + H_3^+ \rightarrow 3H$	$\beta_3(3H)$	
	$\beta_3 = \beta_3(H_2 + H) + \beta_3(3H)$ $= 4 \times 10^{-6} T^{-\frac{1}{2}} cm^3/s$	4

Table A. (contd.)

Reaction	Rate	Reference
Charge exchange		
(A15) $H_2^+ + H \rightarrow H_2 + H^+$	$K_1 = 6 \times 10^{-10} cm^3 s^{-1}$	5
Ion-Molecule reaction		
(A16) $H_2^+ + H_2 \rightarrow H_3^+ + H$	$K_2 = 2 \times 10^{-9} cm^3 s^{-1}$	6

† $\zeta_p(H)$ is the primary ionization rate for atomic H per H atom. The mean energy of the primary electrons in A3-A7 is $\sim$ 20 eV. The rates are slightly composition dependent, but usually by no more than 10-20%.

* Theoretical estimate. In view of the fact that many measured dissociative recombination rates are much larger, e.g. $\beta_3 \sim 10^2 \beta_2$, we have considered this possibility for β_2 in the text of Appendix A.

References:

1. Glassgold and Langer (1973b)
2. Spitzer (1968)
3. Dubrovskii and Ob'edkov (1967)
4. Leu, Johnson, and Biondi (1973)
5. deJong (1972)
6. Neynaber and Trujillo (1968)

FIGURE CAPTIONS

1. Upper part (a): Total grain cross-section per gas atom as a function of wavelength based on (7) and far UV extinction measurements. For the typical star we use $\sigma_{gr}\xi_{gr}(V) = 5.53 \times 10^{-22} cm^2$, i.e. $A_V = N(5/3 \times 10^{21} cm^{-2})^{-1}$. For ζ Oph, we use $A_V = 3E(B-V) = 0.96$, and $N = 1.2 \times 10^{21} cm^{-2}$. Lower part (b): Various models for the UV interstellar radiation field. The solid horizontal bars are Habing's upper and lower limits for the solar vicinity based on an albedo of 0.9 and 0, respectively (Habing, 1968). The broken horizontal line is Habing's recommended value for a typical point in the interstellar medium. The broken horizontal line (1) $u = 3 \times 10^{-17}$ ergs/cm^3 Å is an extrapolation of Lillie's measurements above 2000 Å, and represent a kind of lower limit to the far UV field. The dash curve (2) is an interpolation on Habing's values. Curve (3) is based on Jura's (1974) calculation, (open circles); the dash portion is an extrapolation. Curve (4) is based on the work of Witt and Johnson (1973) (solid points); the dash portion is a rather arbitrary extrapolation to shorter wave lengths, and represents a kind of upper limit to the far UV field.

2. Effect of varying Doppler width parameter b_D for "small" column densities. The upper left curves give the fractional column density of H_2, $F = 2N[H_2]/N$ and the lower right the column density of CI vs. $N = N[H] + 2N[H_2]$. The parameters for the dash curve ($b_D = 4$ km/s) are the common parameters listed in Table 2.

3. Effect of varying the factor c_{cont} in Eq. (22). The upper left curves give the fractional abundance F of H_2, and the lower curves the column density $N[CI]$ of CI vs. N. The parameters for the dash curve ($c_{cont} = 3$) are listed in Table 2.

4. Effect of varying pressure p_o. The upper left curves give the fractional column density of H_2, $F = 2N[H_2]/N$ and the lower right the column density of CI vs. $N = N[H] + 2N[H_2]$. The parameters for the dash curve are the common parameters listed in Table 2. The labels attached to the F curves are mean temperatures.

5. Densities n(H), $n(H_2)$, and n for the standard parameters of Table 2 (top), and temperature T for the 4 calculations in Fig. 3 (bottom) vs. N.

6. Effect of varying the cosmic ray ionization rate. The explanation of the format of these curves is the same as in Fig. 3. $\zeta_p(H)$ is the primary rate for atomic H; the total rate for H and the rates for H_2 are listed in Table A of the Appendix. Note that the curve for F when $\zeta = 10^{-18}s^{-1}$ has not been drawn since it is practically indistinguishable from that for $\zeta = 10^{-17}s^{-1}$. The labels on the upper and lower curves are the mean temperatures and electron densities, respectively.

7. Effect of varying the relative C abundance $\xi(C)$. The explanation of the format of these curves is the same as in Fig. 3. The labels attached to the $N[CI]$ curves are mean temperatures. The curve for $\xi(C) = 4 \times 10^{-4}$ corresponds to the solar abundance.

8. Results for the four interstellar UV radiation fields plotted in Fig. 1(b). The explanation of the format of these curves is the same as in Fig. 3. The labels attached to the F curves are mean temperatures.

9. Effect of variation of the rate constant for H_2 formation on grains. The explanation of the format of these curves is the same as in Fig. 4. The $N[CI]$ curve for $R_1 = 5 \times 10^{-18}cm^3s^{-1}$ has not been plotted because it is practically indistinguishable from that for $R_1 = 10^{-17}cm^3s^{-1}$.

10. Effect of simultaneously increasing p_o and I by a factor of 2 and of 5. The shape of the radiation field is that of the Habing flux I_2 in Fig. 1. The dash curve is for the standard parameters of Table II. The labels attached to the F curves at the top are the mean temperature $\overline{T}$ and the mean density $\overline{n}$, and to the $N[CI]$ curves at the bottom the mean electron density. Note the expanded scale relative to the previous figures.

11. The total (solid line) and 3 major (dash curves) heating rates as a function N. The upper part (a) refers to the standard parameters of Table II; the lower part involves changing the photoelectron heating efficiency from $\overline{y} = 0.1$ to $\overline{y} = 0.2$. The curves for dissociative heating are not included because they represent only a few percent of the heating.

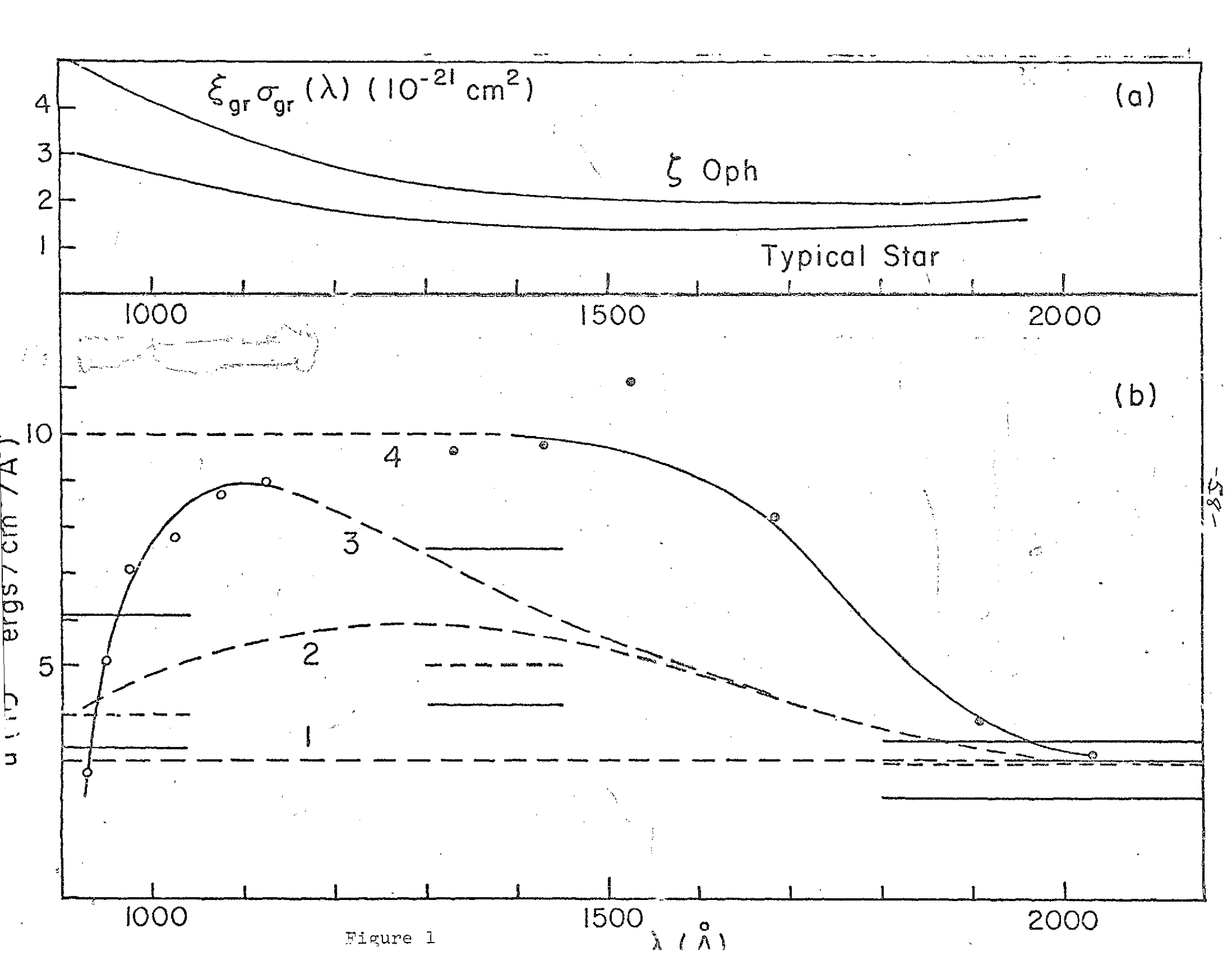
$\xi_{gr}\sigma_{gr}(\lambda)$ (10^{-21} cm^2)
(a)
ζ Oph
Typical Star
4
3
2
1
1000
1500
2000
(b)
10
5
4
3
2
1
ergs/cm²/Å)
1000
1500
2000
λ (Å)

Figure 1

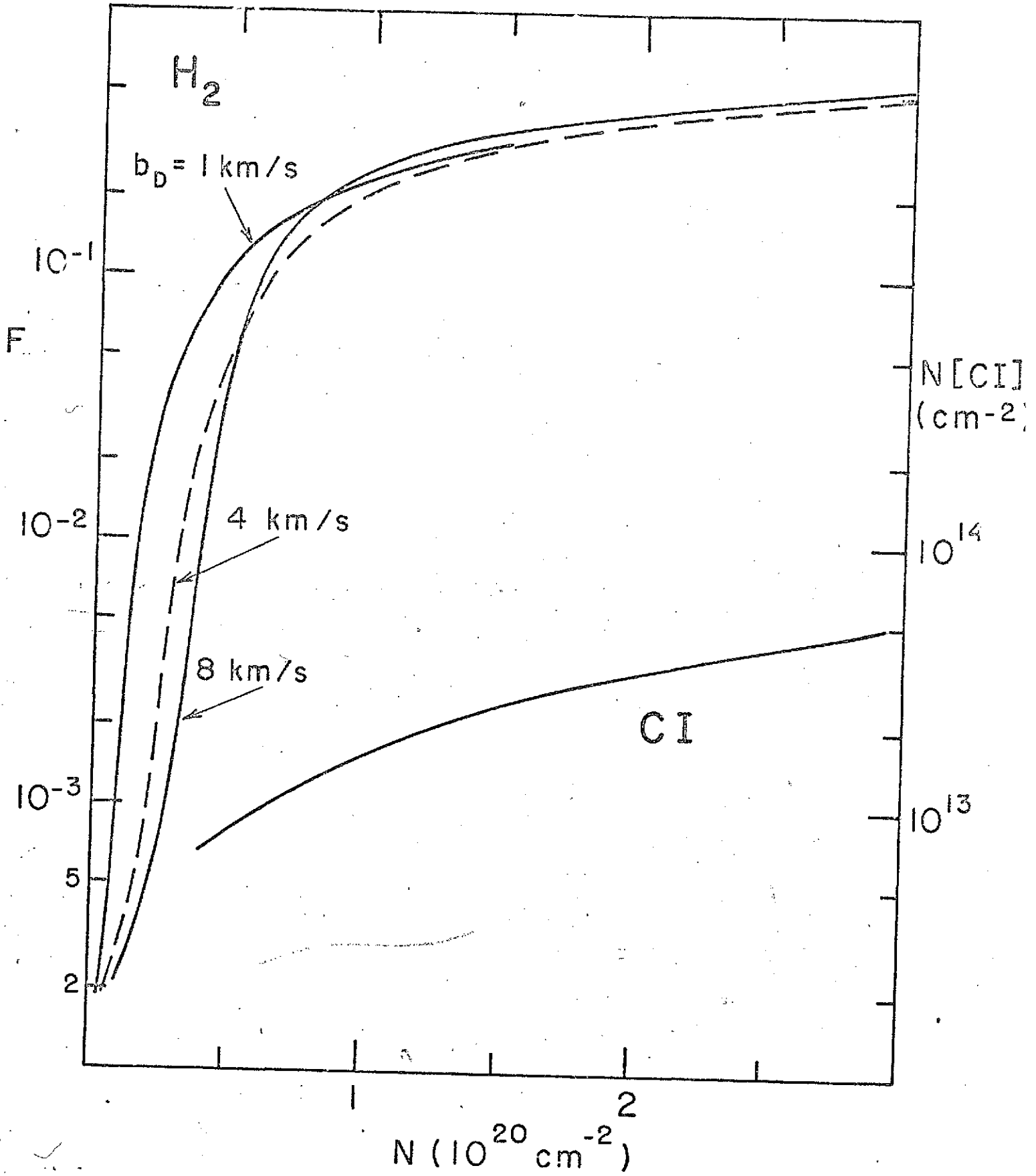
H2
b_D = 1 km/s
4 km/s
8 km/s
CI
F
10^-1
10^-2
10^-3
5
2
1
2
N (10^20 cm^-2)
N[CI] (cm^-2)
10^14
10^13

Figure 2

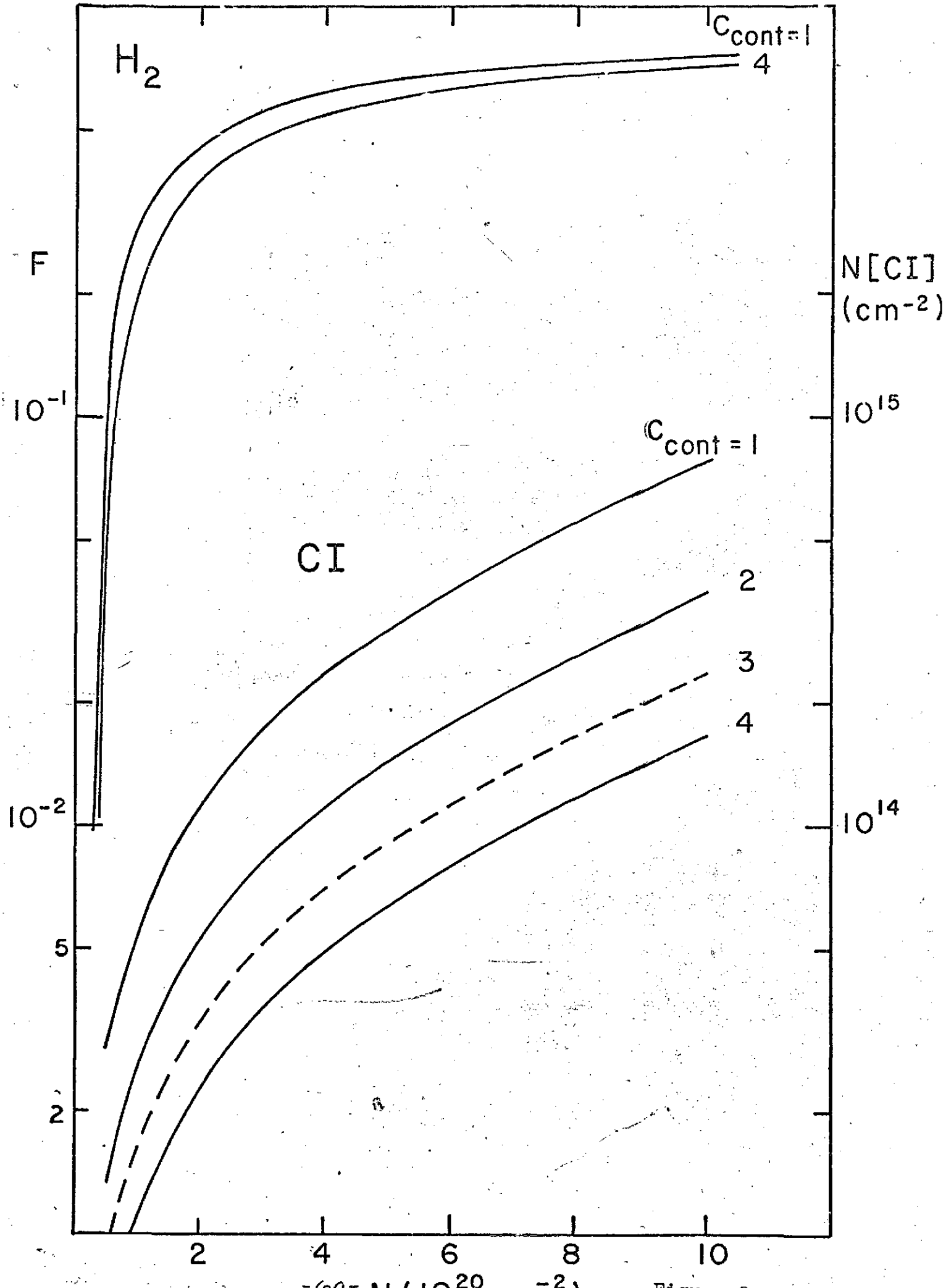
H_2
$C_{cont=1}$
4
F
10^{-1}
10^{-2}
5
2
N[CI]
(cm^{-2})
10^{15}
10^{14}
$C_{cont=1}$
CI
2
3
4
2
4
6
8
10
$N(10^{20} cm^{-2})$

Figure 3

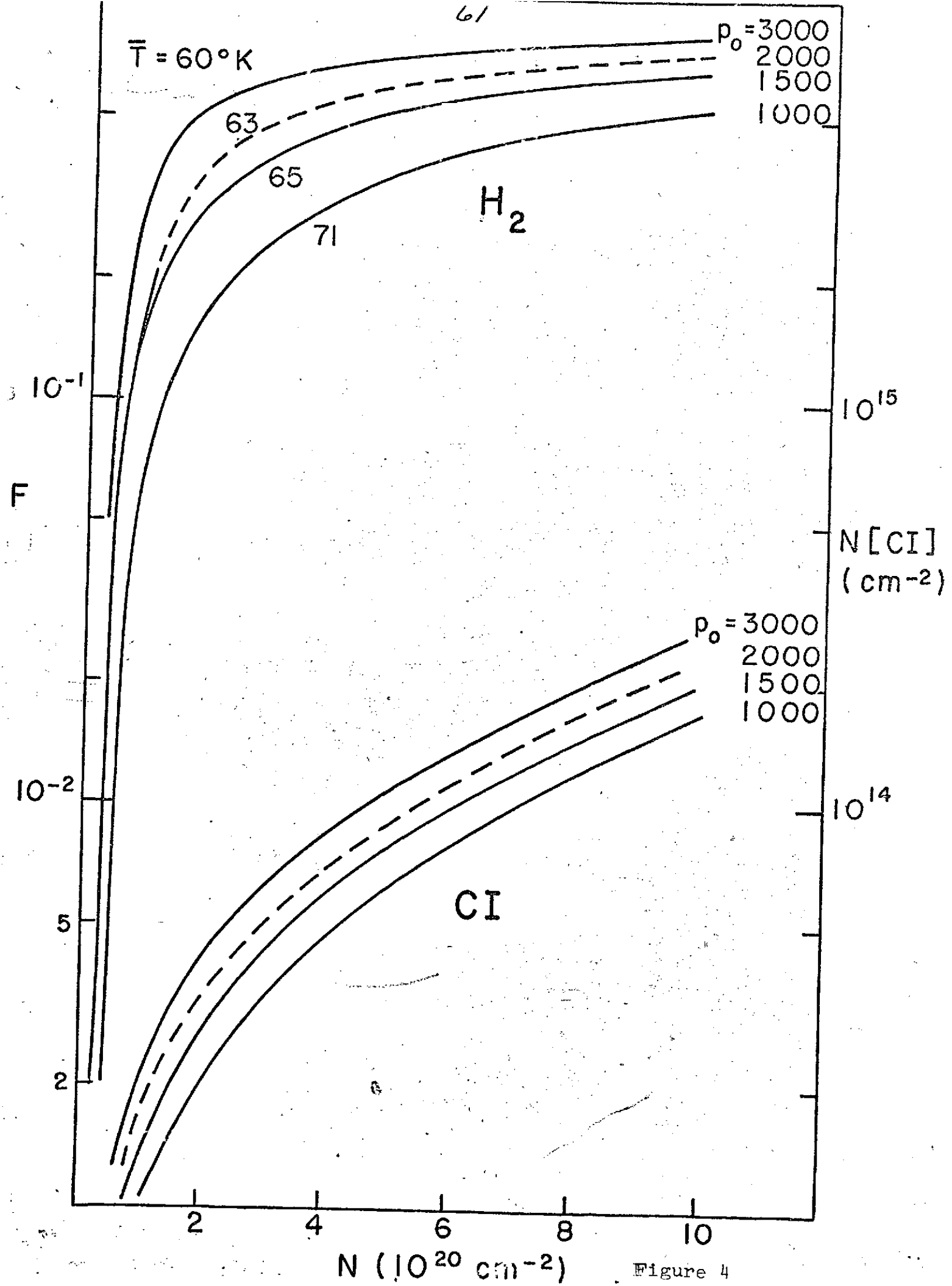
$\bar{T}$ = 60° K
p_o = 3000
2000
1500
1000
63
65
71
H_2
10^{-1}
F
10^{15}
N[CI]
(cm^{-2})
p_o = 3000
2000
1500
1000
10^{-2}
10^{14}
CI
5
2
2
4
6
8
10
N (10^{20} cm^{-2})

Figure 4

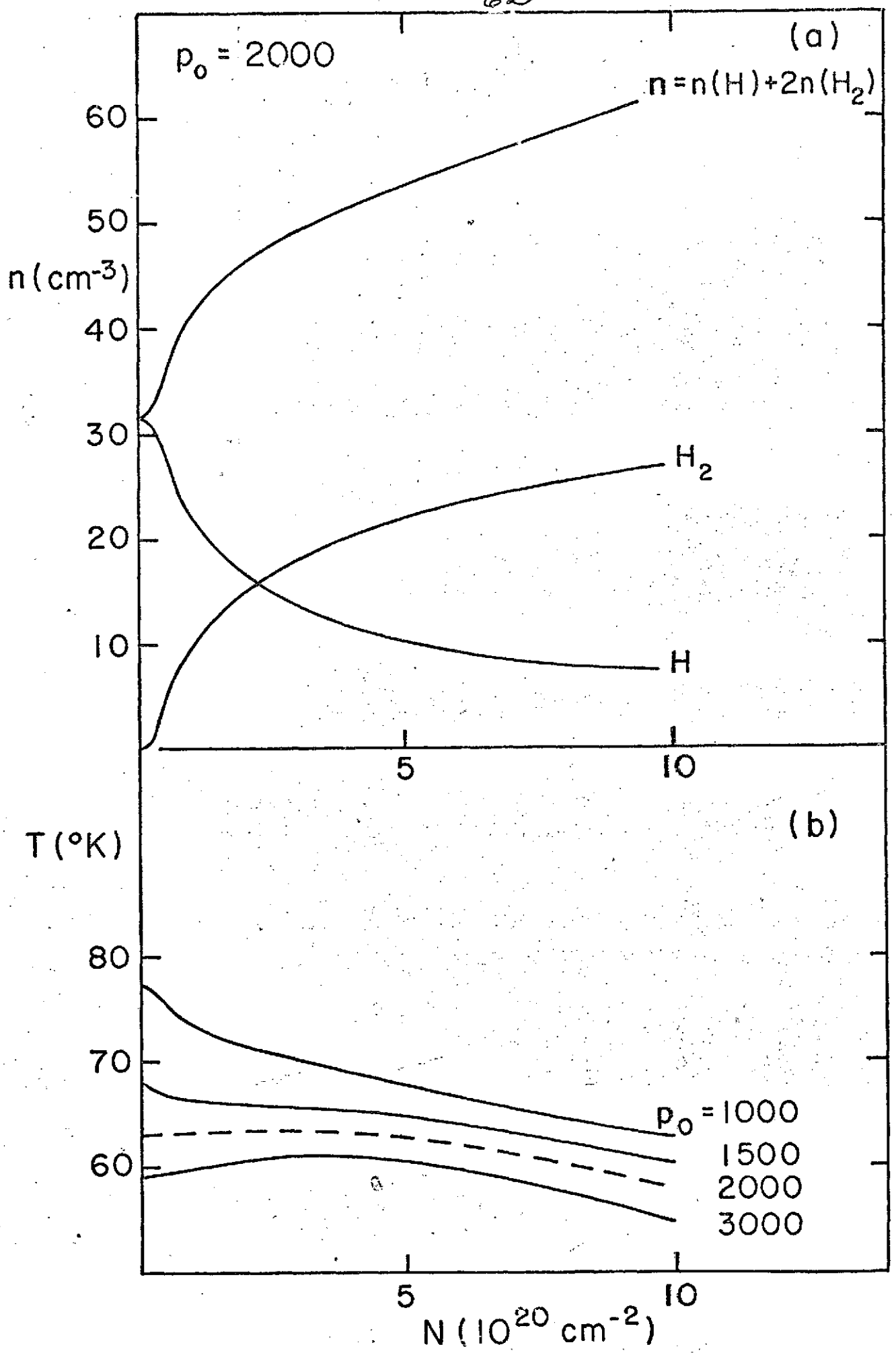
(a)
p_o = 2000
n = n(H) + 2n(H_2)
n (cm^{-3})
60
50
40
30
20
10
H_2
H
5
10
(b)
T (°K)
80
70
60
p_o = 1000
1500
2000
3000
5
10
N (10^{20} cm^{-2})

Figure 5

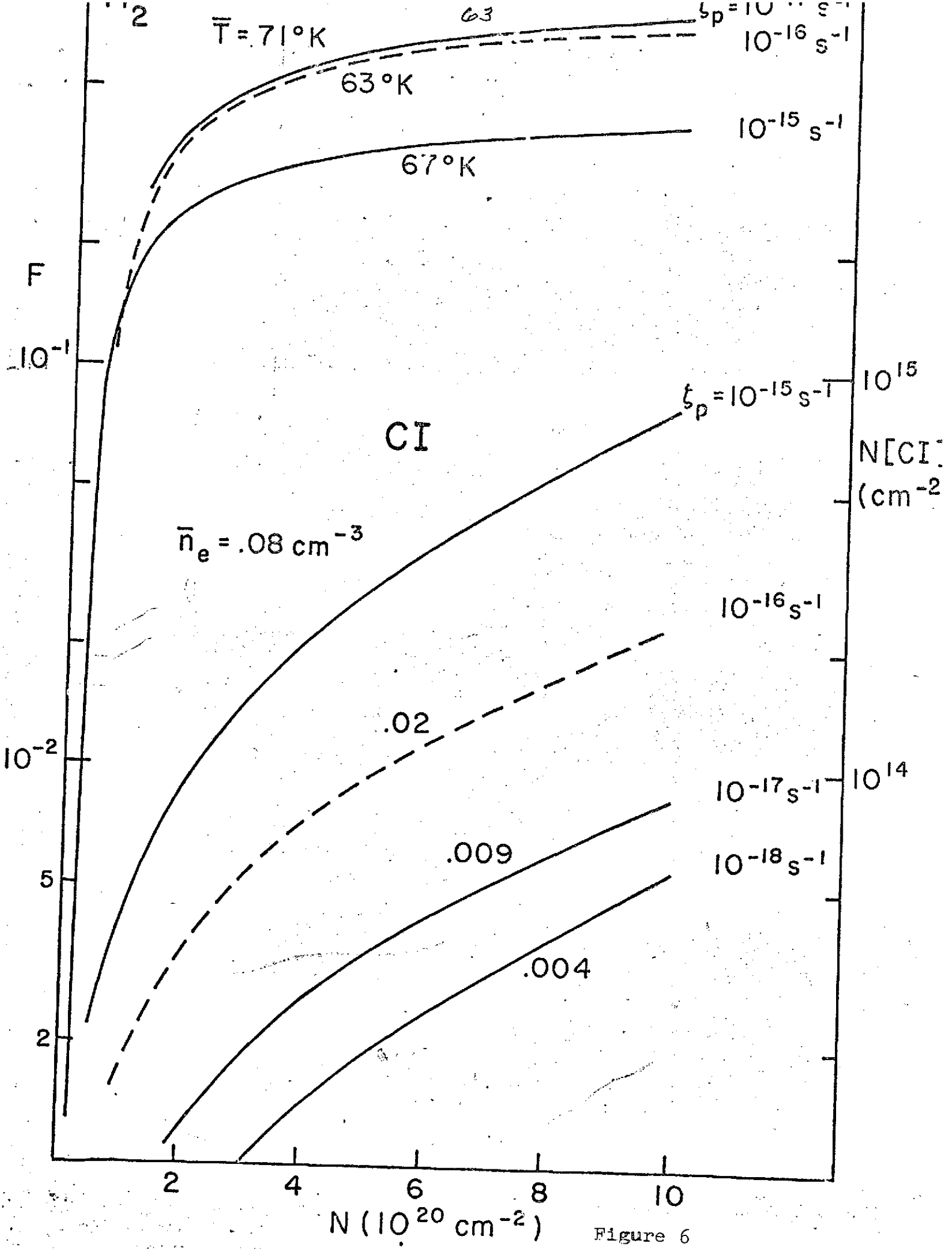
T = 71°K
63°K
67°K
$\zeta_p = 10^{-16}$ s^{-1}
10^{-15} s^{-1}
F
10^{-1}
10^{-2}
5
2
CI
$\zeta_p = 10^{-15}$ s^{-1}
$\bar{n}_e = .08$ cm^{-3}
10^{-16}s^{-1}
.02
10^{-17}s^{-1}
.009
10^{-18}s^{-1}
.004
10^{15}
10^{14}
N[CI]
(cm^{-2}
2
4
6
8
10
N (10^{20} cm^{-2})

Figure 6

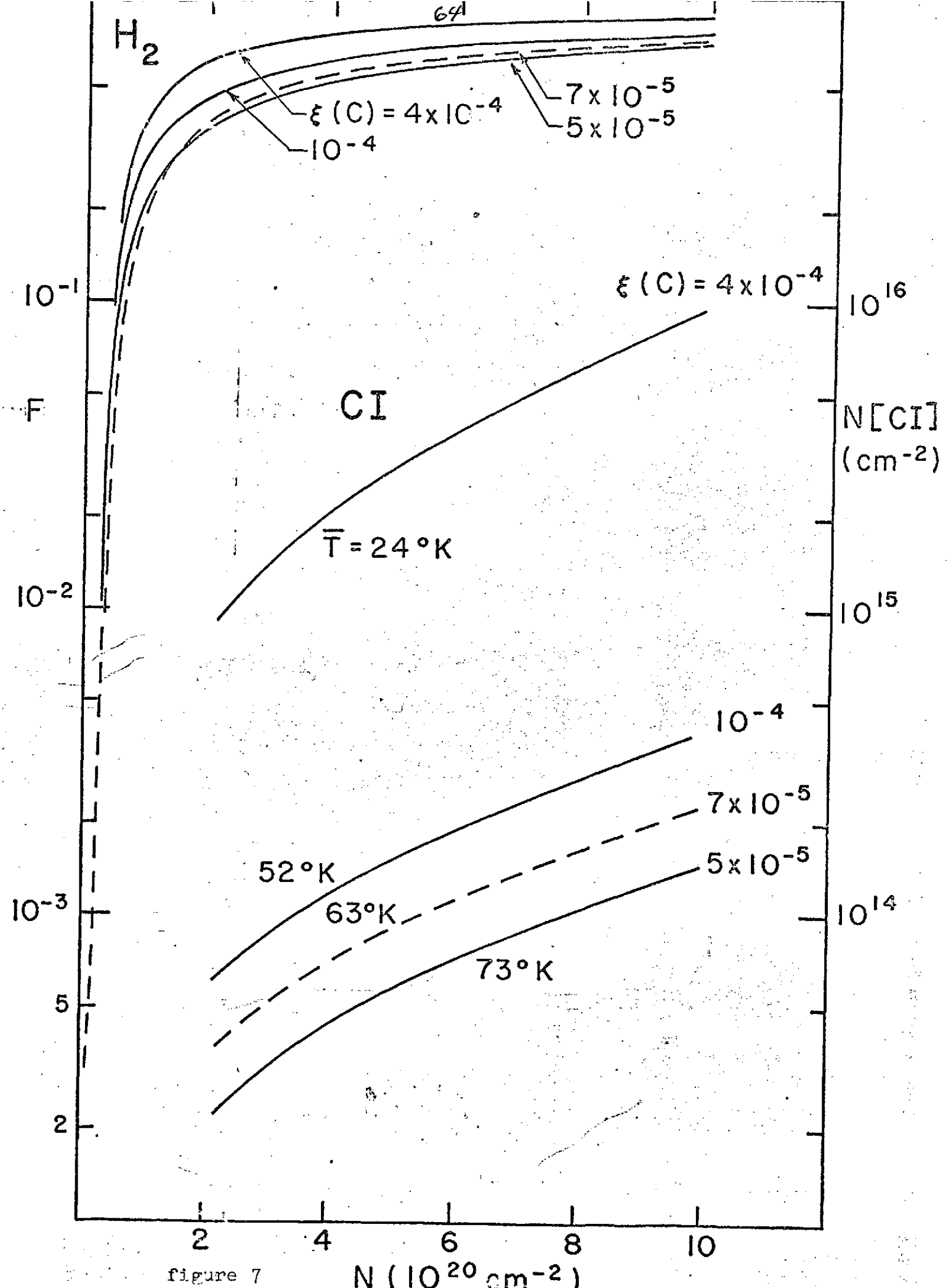
64
H2
ε (C) = 4x10-4
10-4
7x10-5
5x10-5
10-1
10-2
10-3
5
2
F
CI
ε (C) = 4x10-4
T̄ = 24°K
10-4
7x10-5
5x10-5
52°K
63°K
73°K
10^16
10^15
10^14
N[CI]
(cm-2)
2
4
6
8
10
N (10^20 cm-2)

figure 7

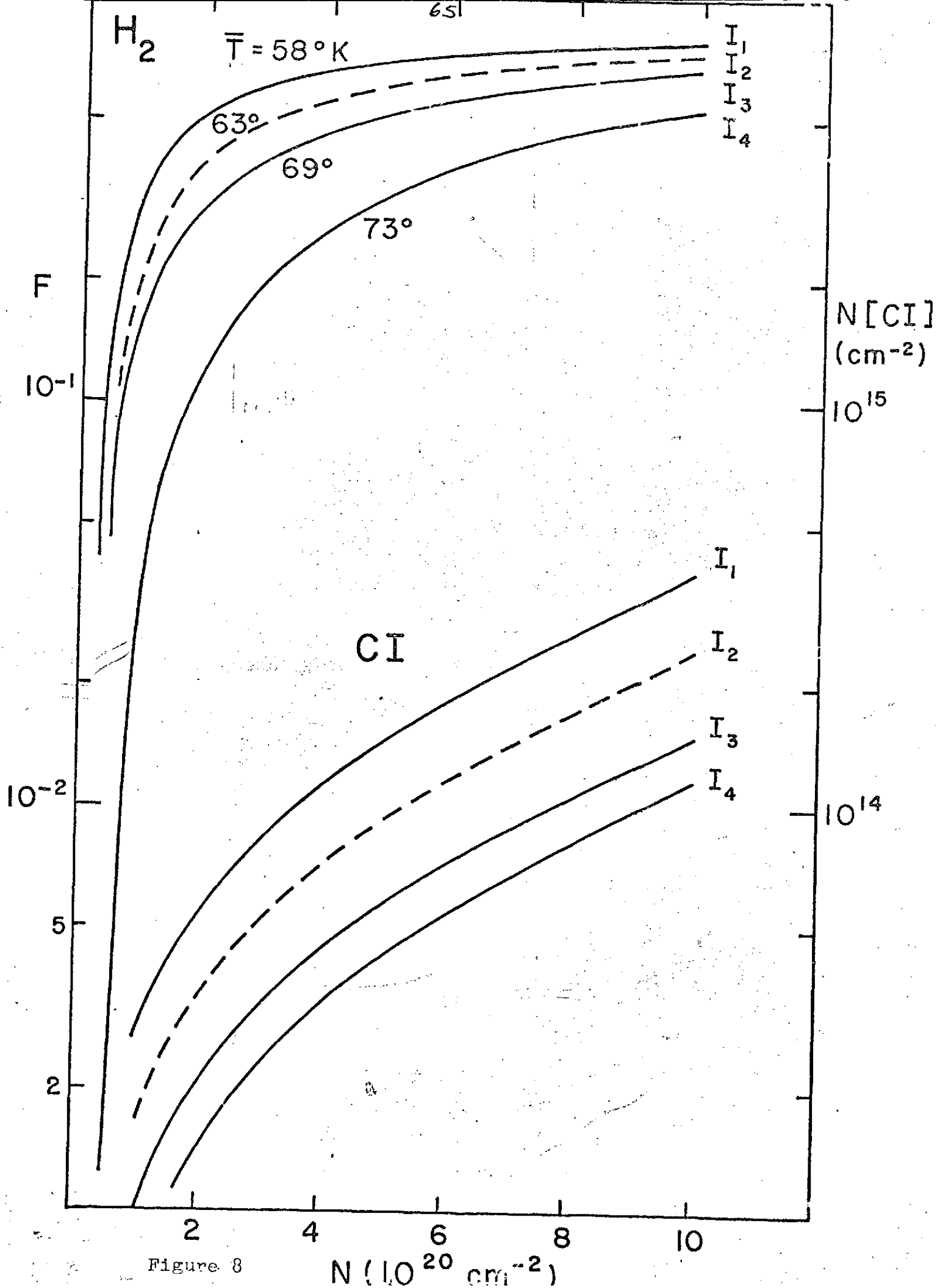
H2
T̄ = 58°K
I1
I2
I3
I4
63°
69°
73°
F
10-1
10-2
5
2
N[CI]
(cm-2)
10^15
10^14
CI
I1
I2
I3
I4
2
4
6
8
10
N (10^20 cm-2)

Figure 8

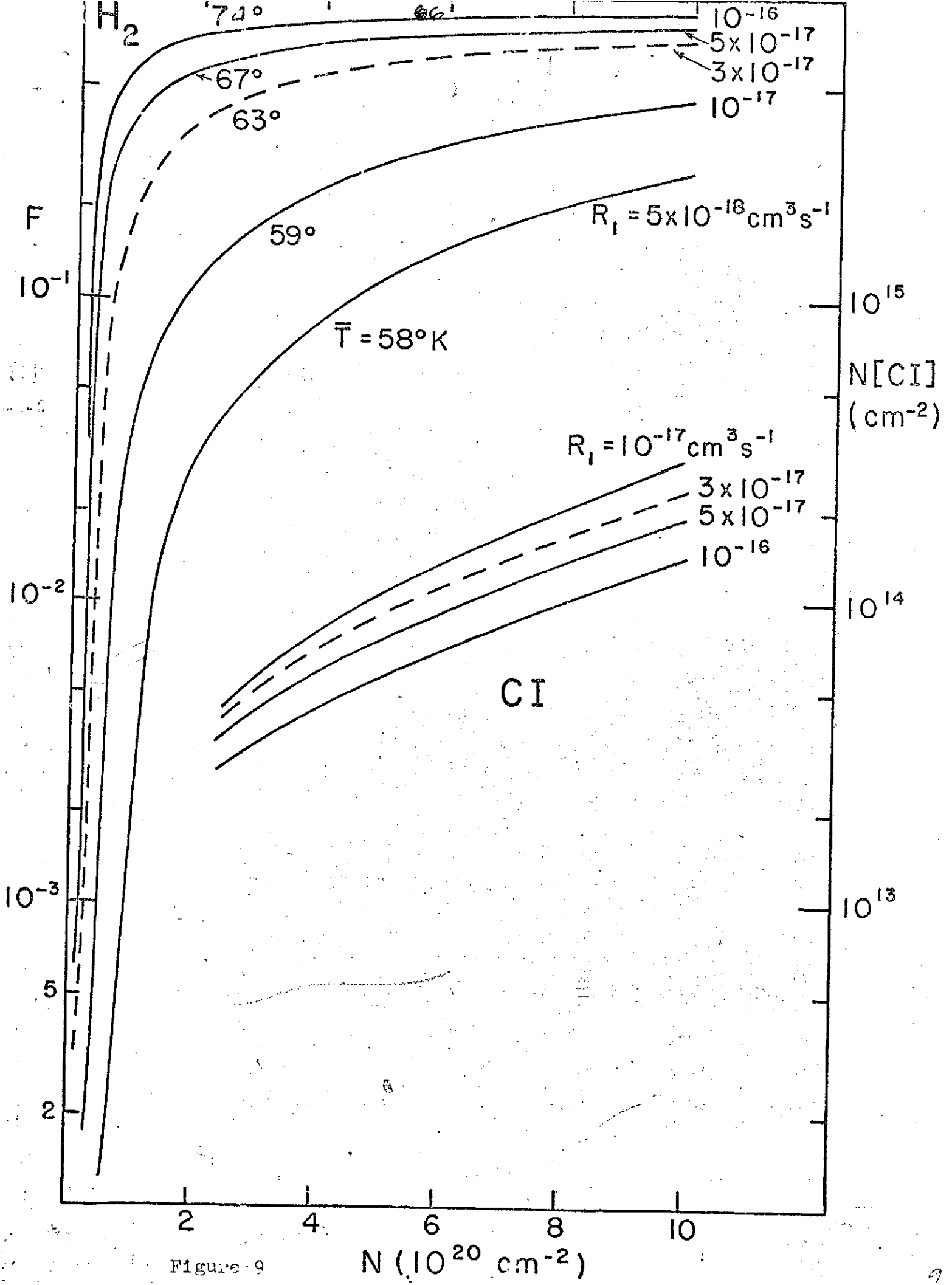
H2
71°
66'
10-16
5x10-17
3x10-17
67°
63°
10-17
F
59°
R1 = 5x10-18cm3s-1
10-1
T̄ = 58°K
10^15
N[CI]
(cm-2)
R1 = 10-17cm3s-1
3x10-17
5x10-17
10-16
10-2
10^14
CI
10-3
10^13
5
2
2
4
6
8
10
N (10^20 cm-2)

Figure 9

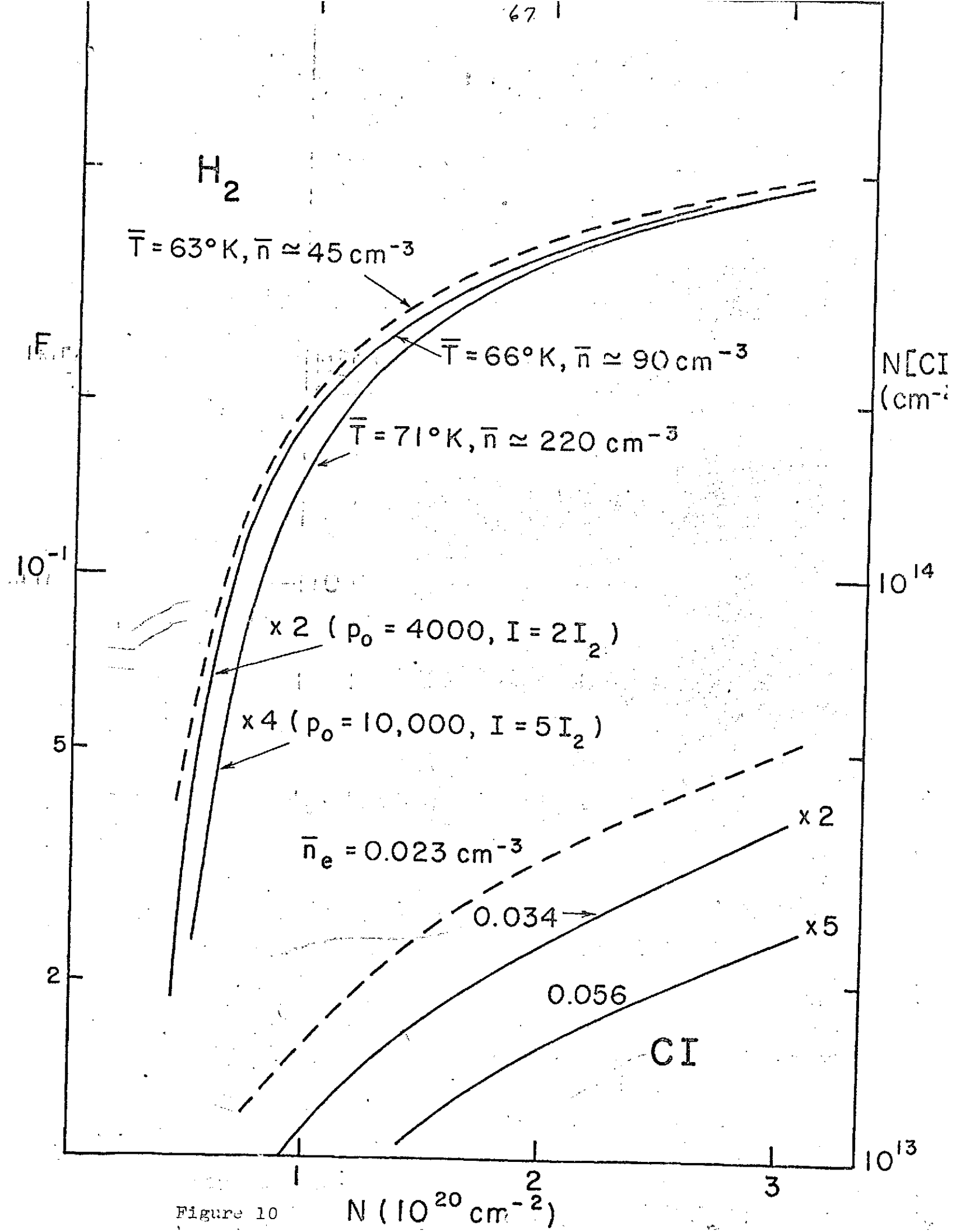
H2
T̄ = 63°K, n̄ ≃ 45 cm⁻³
T̄ = 66°K, n̄ ≃ 90 cm⁻³
T̄ = 71°K, n̄ ≃ 220 cm⁻³
x 2 (p₀ = 4000, I = 2I₂)
x 4 (p₀ = 10,000, I = 5I₂)
n̄e = 0.023 cm⁻³
0.034
0.056
x 2
x5
CI
10⁻¹
5
2
10¹⁴
10¹³
1
2
3
N (10²⁰ cm⁻²)

Figure 10

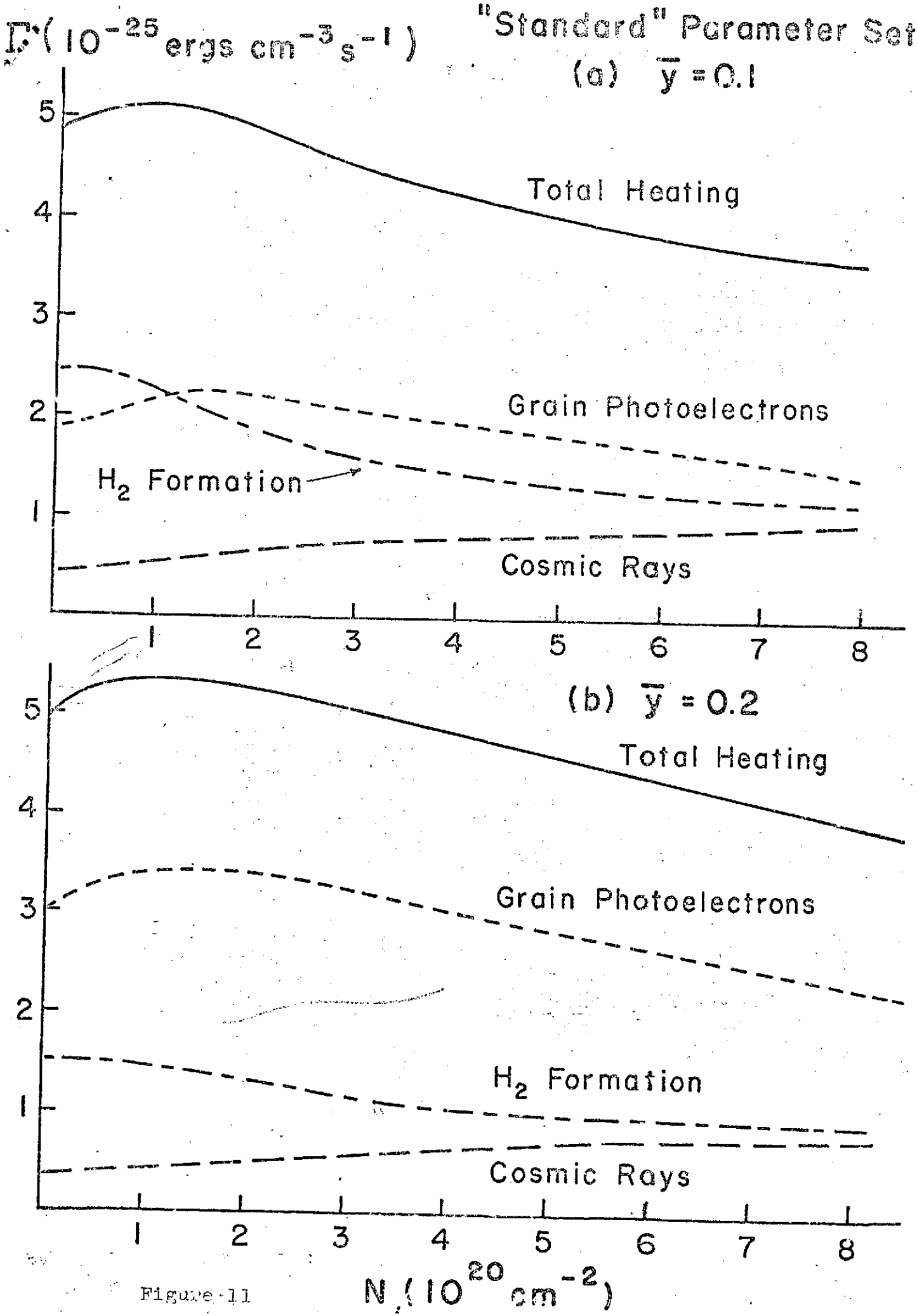
Γ(10⁻²⁵ ergs cm⁻³ s⁻¹)
"Standard" Parameter Set
(a) ȳ = 0.1
Total Heating
Grain Photoelectrons
H₂ Formation
Cosmic Rays
(b) ȳ = 0.2
Total Heating
Grain Photoelectrons
H₂ Formation
Cosmic Rays
N(10²⁰ cm⁻²)

Figure 11